Evaluation of poly(vinyl alcohol) cryogel as viscoelastic reconstruction graft for the ascending aorta

by

Christopher Zikry

Department of Biomedical Engineering
McGill University, Montreal

February 2019

A thesis submitted to McGill University in partial fulfillment of the requirements of the degree of Master of Engineering

Abstract

The ascending aorta is subject to high-pressure, pulsatile flow exiting the aortic valve from the left ventricle. Biomechanical properties of the ascending aorta are responsible for two primary objectives at each heartbeat: (1) distending and contracting to convert pulsatile flow into steady flow, and (2) dissipating energy from the peak of flow to preserve the local vascular wall and protect peripheral vasculature and organs from damage. These objectives can be roughly attributed to the elastic and viscous properties, respectively, of the viscoelastic aorta. Surgical intervention is required in cases when the aortic wall is unable to maintain these responsibilities (aneurysm) or eventually undergoes mechanical failure (dissection or rupture). Diseased tissue is traditionally replaced by a textile vascular conduit known as Dacron. Although Dacron maintains long-term patency in large arteries, its dissimilar mechanical properties to the surrounding tissue inhibit the ascending aorta's ability to fulfill its biomechanical objectives. Investigation into viable replacements have largely focused on matching compliance (elasticity) of aortic tissue. This work examines the use of poly(vinyl alcohol) cryogel (PVA-C) as a substitute material to mimic both the ascending aorta's elastic and viscous properties.

Various PVA-C compositions were formed for examination. Ascending aorta, PVA-C, and Dacron underwent loading-unloading biaxial tensile tests, stress relaxation, and dynamic mechanical analysis. Incremental modulus and energy loss were determined from biaxial tensile tests. Fung's quasi-linear viscoelasticity (QLV) theory was applied to stress relaxation curves and parameters determined. Complex modulus (E^*) and loss factor ($tan\ \delta$) across [0.1 - 20] Hz were assessed. Incremental modulus of 20% PVA-C matches aortic tissue at high (45%) strain. Energy loss increased with PVA concentration and 10% PVA-C closely matched energy loss of healthy tissue. Stress relaxation responses confirmed elastic and viscous parameters from biaxial tensile tests. QLV parameters of PVA-C formulations were within range of healthy tissue, with 20% PVA-C exhibiting the most resemblance. Magnitude and frequency-dependence of 15% PVA-C complex modulus matched aortic tissue, while all PVA-C formulations were within range of loss factor in healthy tissue of all frequencies tested. In all experiments, Dacron repeatedly exhibited increased storage and loss moduli in comparison to the other groups. These data suggest PVA-C should be considered in developing novel ascending aorta grafts that not only restore flow, but also rectify their biomechanical functions.

Résumé

L'aorte ascendante est sujette à un flux pulsatile à haute pression sortant de la valve aortique par le ventricule gauche. Les propriétés biomécaniques de l'aorte ascendante sont responsables de deux objectifs principaux à chaque battement de cœur: (1) se distendre et se contracter pour convertir un flux pulsatile en flux constant, et (2) dissiper de l'énergie du pic du flux pour préserver la paroi vasculaire locale et protéger le système vasculaire périphérique et les organes contre les dommages. Ces objectifs peuvent être approximativement attribués aux propriétés élastiques et visqueuses de l'aorte viscoélastique. Une intervention chirurgicale est nécessaire dans les cas où la paroi aortique est incapable d'assumer ses responsabilités (anévrisme) ou subit éventuellement une défaillance mécanique (dissection ou rupture). Le tissu malade est traditionnellement remplacé par un conduit vasculaire textile appelé Dacron. Bien que le Dacron préserve une perméabilité à longue durée dans les grandes artères, ses propriétés mécaniques dissemblables par rapport au tissu environnant entravent la capacité de l'aorte ascendante à maintenir ses objectifs biomécaniques. L'enquête sur les remplacements viables s'est largement concentrée sur lextensibilité correspondante au tissu aortique. Cette thése étudie l'utilisation du cryogel d'alcool polyvinylique (PVA-C) comme matériel de substitution pour imiter les propriétés élastiques et visqueuses de l'aorte ascendante.

Diverses compositions de PVA-C ont été formées pour cet examen. L'aorte ascendante, le PVA-C et le Dacron ont subi des tests de traction biaxiale avec chargement et déchargement, une relaxation des contraintes et une analyse mécanique dynamique. Le module incrémental et la perte d'énergie ont été déterminés à partir d'essais de traction biaxiaux. La théorie de la viscoélasticité quasi-linéaire (QLV) de Fung a été appliquée aux courbes et paramètres de relaxation de contrainte. Le module complexe ($E*$) et le facteur de perte ($tan\,\delta$) à travers [0,1 - 20] Hz ont été évalués. Le module incrémental de 20% PVA-C correspond au tissu aortique à une déformation haute (45%). La perte d'énergie augmentait avec la concentration de PVA et 10% PVA-C correspondait à une perte d'énergie similaire à celle d'un tissu sain. Les réponses à la relaxation de contrainte ont confirmé les paramètres élastiques et visqueux des essais de traction biaxiale. Les paramètres QLV des formulations de PVA-C se situaient dans la gamme des tissus sains, avec 20% PVA-C présentant le plus de similitude. Dépendance de la magnitude et de la fréquence des tissus aortiques appariaient avec un module complexe à 15% PVA-C, alors que toutes les formulations de PVA-C se situaient dans la gamme du facteur de perte dans les tissus sains de toutes les fréquences testées. Dans toutes les expériences, Dacron a présenté à plusieurs reprises des modules de conservation et de perte accrus par rapport aux autres groupes. Ces données suggèrent que le PVA-C devrait être pris en compte dans le développement de nouvelles greffes d'aorte ascendante qui non seulement rétablissent le flux, mais également rectifient leurs fonctions biomécaniques.

Acknowledgments

I would like to thank my supervisor, Professor Rosaire Mongrain, for his guidance and support. His ambition to fill voids in scientific knowledge has propelled this project. Every meeting introduced new questions and pushed me further in searching for answers. Additionally, I would like to acknowledge my co-supervisors, Dr. Raymond Cartier and Dr. Gilles Soulez, both of whom have provided invaluable clinical knowledge and critical comments.

This work would not have been possible without the aid of Professor Richard Leask, who ensured my access to testing equipment. I am grateful for his allowing me to conduct experiments in his laboratory and flexibility with my time-intensive experiments and meeting my deadlines. Furthermore, I must acknowledge my friend and colleague, Alex Emmott. His patience in installing the equipment and training allowed the project to succeed on a tight schedule. His expertise in biaxial tensile testing and useful conversations were indispensable in collecting interpretable data.

I would like to especially thank Dr. Ismail El-Hamamsy, Michaël Tousch, and the rest of the team involved in providing the aortic tissue used in this study. I am indebted to Vanessa Hertig for her help in coordinating tissue collection and obtaining histological images. She helped me navigate Montreal Heart Institute and her presence there was crucial when I could not be at two places at once. I am incredibly grateful for her time and selfless effort through this project.

I cannot express enough gratitude to Dr. Paul Khairy and Ms. Nadine Yared for greeting me with open arms and giving me a second home in Montreal. Their support and encouragement helped me forget my research struggles. I would also like to thank Drs. Ramez and Marie-Thérèse Khairy for all our heartening conversations. Each moment we shared was renewing and motivating in attacking every problem I faced. Words cannot convey the appreciation I have for the Khairy and Walsh families, without whose support I could not have completed this work.

Lastly, I must sincerely thank my parents, Sameh and Mona, for their unconditional love and unwavering patience. Although miles away, they remained beside me during struggle and triumph as I reached the end.

Contents

List of Figures

List of Tables

Chapter 1

Introduction

1.1 Motivation

The prevalence of cardiovascular disease has propelled scientific research, revolutionary design, and surgical innovation in the field. The investigation of arterial tissue biomechanics has been of particular relevance in classifying tissue viability over repeated cyclic stresses. Biomechanical parameters of arterial tissue have evolved as quantitative measures of pathophysiological progression. These parameters will be used to describe the *in vivo* behavior of the ascending aorta. The aorta is the largest blood vessel, delivering oxygenated blood to the circulatory system. The mechanical properties of the ascending aorta determine its ability to withstand repeated stresses at high pressure and to distend according to flow demands. Standard aortic replacement grafts poorly replicate the native function of healthy tissue. While ideal artificial vessels will replace the biological and biomechanical roles of dynamic, living tissue, the focus of this research is solely understanding the mechanical behavior of aortic tissue and its viable replacements. *Ex vivo* tensile testing has been widely used to examine biological soft tissues and material models have been developed accordingly. These tools are implemented in the research presented here to evaluate human ascending aortic tissue, commercial Dacron grafts, and a potential graft replacement designed from poly(vinyl alcohol). The goal of this project is to develop a polymeric material that replicates both elastic and viscous properties of native aortic tissue.

1.2 Objectives

The objectives of this research project are as follows:

Objective 1 To assess the viscoelastic properties of human ascending aorta through stress relaxation and dynamic mechanical analysis (DMA).

Objective 2 To characterize poly(vinyl alcohol) cryogel (PVA-C) formulations based on elastic and viscous properties.

These objectives guide the selection of a novel PVA-C formulation to serve as a material for ascending aorta replacement.

1.3 Thesis Overview

Chapter 2 provides background of the cardiovascular physiology, with intimate focus on the arterial wall's structure as it relates to its function. Chapter 3 details a brief literature review explaining the motivation for and previous approaches considered in designing a novel ascending aortic graft. Bearing particular interest in this study, chemistry of poly(vinyl alcohol) is considered to defend its use as a plausible graft replacement. Chapter 4 describes the experimental methods of PVA-C formation and mechanical characterization protocols. Fung's quasilinear viscoelasticity (QLV) is introduced to characterize each material's nonlinear viscoelasticity. Chapter 5 presents the results from the biaxial tensile, stress relaxation, and frequency sweep tests. Estimations of QLV model parameters are revealed and frequency-dependent behavior is evaluated. Chapter 6 details the significance of the main findings and discusses its contribution to the field in view of current limitations. Future work is suggested. Chapter 7 offers closing thoughts.

Chapter 2

Cardiovascular Physiology

This chapter presents an overview of the structure and function of the cardiovascular system. Biomechanical aspects of the arterial wall are briefly discussed. Instances of aortic wall failure and current interventional strategies are introduced.

2.1 Circulatory System

The circulatory system is a closed-loop consisting of blood vessels entering and exiting the heart. The heart is a four-chamber pump divided into the right and left side. The right atrium receives oxygen-deficient blood from the systemic circuit and the right ventricle pumps this blood through the pulmonary circuit. The left atrium receives oxygen-rich blood from the pulmonary circuit and the left ventricle pumps this blood through the systemic circuit. Figure 2.1 illustrates the pulmonary and systemic circulations in relation to the heart's two sides. The heart is responsible for the transport of blood throughout the body. Blood not only transports oxygen required for metabolism, but also delivers nutrients and removes metabolic waste. Gas exchange occurs in capillaries where reduced blood pressure and flow permit nutrient transfer.

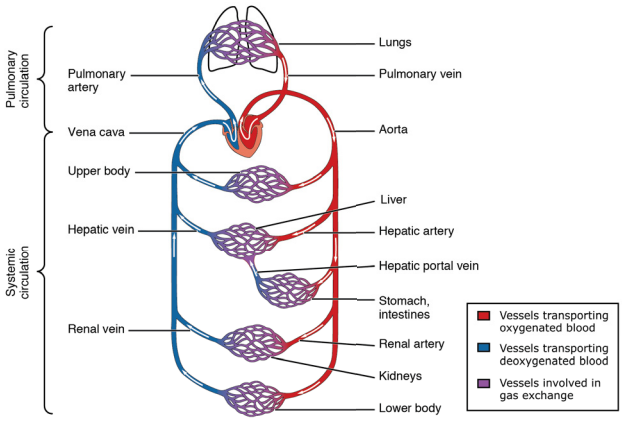

Figure 2.1: The pulmonary and systemic circuits in relation to the heart. Arrows indicate blood flow direction. Colors denote oxygen concentration level [2].

Blood vessels can be further categorized by their flow direction with reference to the heart. Arteries carry blood away from the heart, while veins carry blood towards the heart. In the systemic circulation, arteries transport oxygen-rich blood at high pressure and veins transport oxygen-deficient blood at low pressure. Arteries evolve into arterioles and veins derive from venules at increasing distance from the heart. Capillaries, as small as 10 μm, allow nutrients and metabolic waste to be transported. Arterioles, therefore, are responsible for providing flow resistance not only to facilitate transport in capillaries, but also to protect them from wall damage. Figure 2.2 shows blood pressure levels as blood escapes the left heart and returns to the right heart.

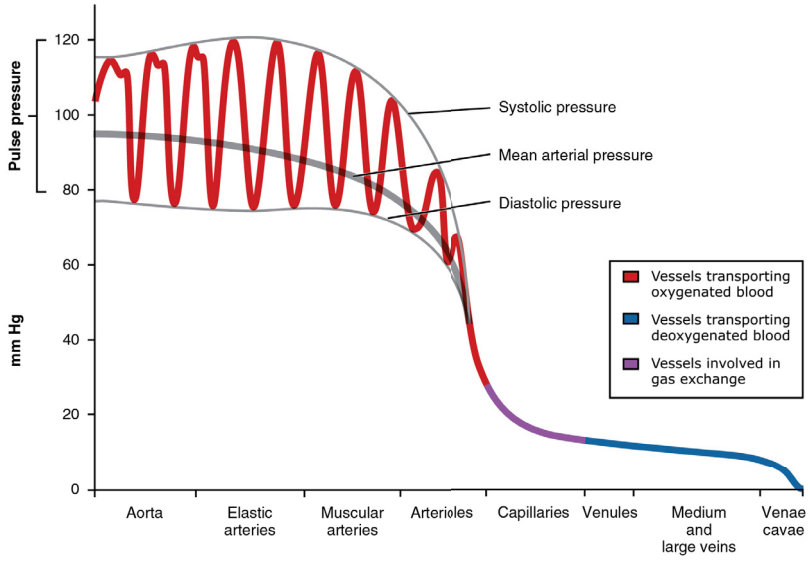

Figure 2.2: Blood pressure drops along the systemic circulation. Colors denote oxygen concentration level [2].

Each vessel type supports a defined role in maintaining circulatory function. Arteries (buffer vessels) relay high-pressure pulsatile flow from the heart, while arterioles (resistance vessels) moderate flow to dampen oscillations as vessel diameter decreases. Conversely, venules and veins (capacitance vessels) serve as blood reservoirs, containing approximately 64% of the systemic blood volume. Following capillary beds, veins are not equipped with the arterial high-pressure to drive flow towards the heart. Valves ensure unidirectional flow in veins to compensate its low-pressure.

The aorta is the largest vessel in the body, initiating at the aortic root and ending at the iliac bifurcation. The thoracic aorta contains sections of the aorta maintained within the thoracic region, namely the aortic root, ascending aorta, aortic arch, and descending aorta, identified in Figure 2.3. The aortic root begins at the aortic valve and ends at the sinotubular junction. The aortic arch distributes oxygenated blood to the brachiocephalic, left common carotid, and left subclavian arteries, which transport blood to the head and arms. The descending aorta extends to the diaphragm, from which the abdominal aorta begins. Arterial biomechanics, and more specifically, biomechanics of the ascending aorta are the focus of this thesis. To further elucidate arterial biomechanical function, the wall microstructure must be considered.

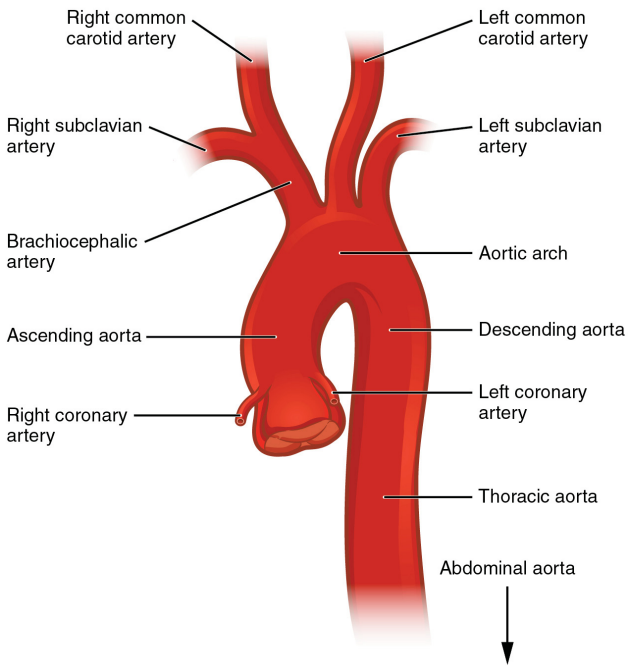

Figure 2.3: Thoracic aorta physiology starts from the aortic valve and ends at the abdominal aorta [91].

2.2 Arterial Wall Structure

The vascular wall is composed of three distinguishable layers: *tunica intima*, *tunica media*, and *tunica adventitia*. While these layers are present in both arteries and veins, the arrangement and relative amount of its constituents vary among vessel type. For the purpose of this study, only arterial wall structure will be considered. Arteries can be subdivided into elastic and muscular. Their subtle, yet discrete structural differences highlight their respective biomechanical functions. Figure 2.4 portrays the constituents organized within each wall layer.

The *tunica intima* is the innermost concentric layer in contact with blood. It lines the vascular wall with an endothelial cell layer over a thin extracellular matrix layer known as the *basal lamina*. Structurally, its biomechanical influence on the global vascular wall is insignificant. However, the endothelium releases vasoactive factors responsible for regulating vascular tone by vasodilation or vasoconstriction [72, 175]. Furthermore, mostly present in large elastic arteries, the *tunica intima* contains a subendothelial layer, composed of smooth muscle cells and a three-dimensional network of collagen and elastic fibers [168]. The *tunica media* is the middle layer and usually the thickest of the arterial wall layers, composed of smooth muscle cells, elastin, and collagen fibrils. The number of elastic laminae decrease further along the arterial system, which differentiate elastic arteries from muscular arteries. Collagen and smooth muscle cells are aligned circumferentially to provide resistance to circumferential loads. Elastic arteries (conducting arteries) allow expansion and offer elastic recoil, while muscular arteries limit expansion and promote vasoconstriction through increased smooth muscle cell content. The *tunica adventitia* is the outermost layer of the vascular

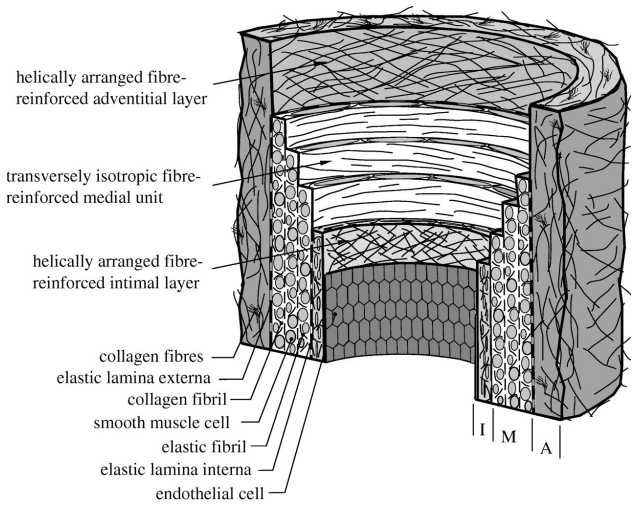

Figure 2.4: Schematic depicting arterial wall architecture. A = *adventitia*, M = *media*, I = *intima*. Reproduced from [73] with permission of Royal Society.

wall, containing mostly collagen fibers, which provides stability to the distending structure. In large elastic arteries, the *adventitia* constitutes 10% of the vascular wall, while it approaches half of the vascular wall thickness in muscular arteries [168].

In summary, elastic arteries are closest to the heart and must have thick walls to withstand the highest pressure in the circulatory system. Furthermore, they contain the highest amount of elastin to allow radial expansion. On the other hand, muscular arteries contain more smooth muscle as expansion is not critical at lower pressure. Elastic and muscular arteries share similar structures and can sometimes be indistinguishable. Elastic arteries gradually transition into muscular arteries as pressure decreases further from the heart.

2.3 Biomechanics of the Arterial Wall

Mechanical properties of composite materials reflect those of each of its components. The relative composition and geometric arrangement of each constituent determine the local and global properties of the arterial wall. Elastin, collagen, and smooth muscle are organized heterogeneously within its three layers to maintain physical equilibrium and provide structural integrity with every heartbeat. The arterial arrangement of all individual wall layers qualifies the constituted wall as cylindrically orthotropic, by which circumferential and longitudinal properties are biomechanically distinct [209].

The arterial structure sustains blood pressure by opposing forces [35] involved in allowing diameter increase and maintaining resistive wall tension. Wertheim discovered of most biological soft tissues that stiffness increases more rapidly than its elongation [211]. In 1880, Roy, by incrementally increasing weights on strips of aortic tissue, confirmed that the arterial wall also deviates from Hooke's law [172]. Like Wertheim, he observed a hyperelastic stress response as strain increased. In a no-load configuration (i.e. *ex vivo*), the arterial wall exhibits non-Hookean behavior at large

strains. However, in the physiological pressure-diameter regime, the healthy arterial wall has been estimated as a linear elastic material with negligible error [27, 63, 118, 160, 181, 184].

2.3.1 Elastin

Elastin is responsible for arterial's distensibility at low strain. Purified elastic tissue adheres to Hooke's law until reaching its yield point. Uniaxial [78] and multiaxial [79] testing of purified elastin networks from the porcine thoracic aorta reveals a linear relationship between stress (load) and strain (elongation) for large deformations. Experiments on purified elastin rings from a porcine thoracic aorta [125] and constitutive models of elastinous sheets and tubes [206] maintain this linearity. Microscopic examination of arterial *media*, seen in Figure 2.5, reveals elastin is organized in a spring-like structure, which stretches and recoils with each cardiac cycle. Elastin in arteries stores elastic-strain energy, increasing efficiency of the circulatory closed-loop system [75].

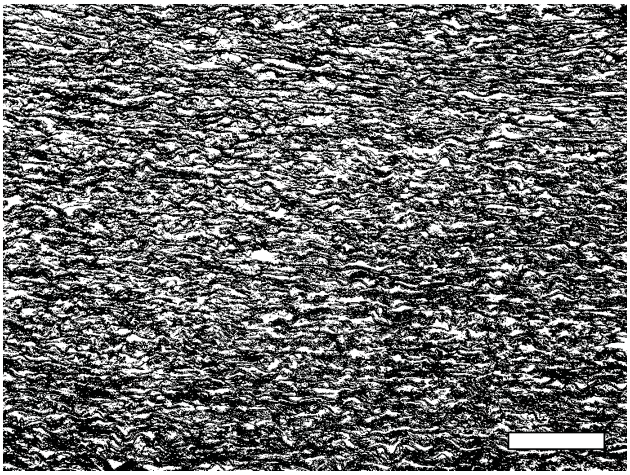

Figure 2.5: Layers of wavy elastinous sheets in *media* of the ascending aorta. Scale bar represents 100 μm.

2.3.2 Collagen

The arterial wall's nonlinear elasticity is attributed to the presence of collagen. Unlike elastin, collagen exhibits an increased stiffness following a linear stress-strain relationship at low strains. Its elastic modulus is orders of magnitude higher than that of elastin [35, 75]. In a study by Roach and Burton, the unique contributions of elastin and collagen in human iliac arteries were identified when inactivated by trypsin and formic acid digestion, respectively [169]. Arterial elastic modulus (stiffness) resembled that of elastin at low strains and that of collagen at high strains. The elastic response of an elastin-collagen composite is illustrated in Figure 2.6.

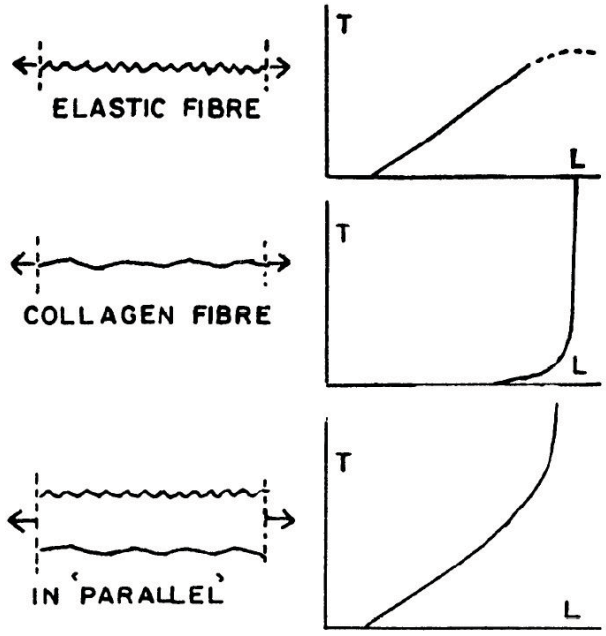

Figure 2.6: Isolated and compound tension-length curves of elastic and collagen fibers. Reproduced from [35] with permission from The American Physiological Society.

The transition between these two regions in the curve represents the recruitment of collagen fibers as strain increased. Thus, at physiological pressures, global load transfers from elastin to collagen. At high pressures, collagen fibers are responsible for reinforcing the distending wall [176]. When arranged in parallel with elastin, the collagen network limits tissue deformation and protects the weaker elastin network [75]. Microscopic examination of elastin and collagen organization in porcine thoracic aortas during biaxial loading reveals fiber engagement transfers from elastin to collagen around 20% strain [44]. All aortic diseases are accompanied with microstructural alterations to the elastin or collagen fibers, which determine the vessel's passive elasticity [194]. In the same way, ageing has irreversible consequences on arterial stiffness through the loss of elastin turnover [55, 95, 178].

2.3.3 Smooth Muscle

Smooth muscle contributes to passive tension of the vascular wall, but is mainly responsible for vascular tone, or active tension in the wall. Activated smooth muscle increases tension at small strains as compared to elastin and collagen alone [90]. At high strains, the non-linear tension caused by elastin and collagen is preserved. Bank et al. isolated the effect of smooth muscle relaxation on the brachial artery *in vivo* by administering nitroglycerin [20]. Relaxed smooth muscle resulted in an increased compliance and decreased elastic modulus at physiological pressure. Increased compliance was reproduced in the descending thoracic aorta of conscious dogs with intravenous infusion of phenylephrine [21, 50]. Elastic modulus was found to increase with smooth muscle activation. Armentano et al. estimated the contribution from elastin, collagen, and smooth muscle

fibers to the wall mechanics of descending thoracic aortas in conscious dogs [12]. Total elastic, viscous, and inertial moduli were quantified in the observed hysteresis loop using a constitutive equation incorporating elastin, collagen, and smooth muscle, as well as nonlinear functions relating muscle activation and collagen fiber recruitment. The effect of smooth muscle activation and pressure on viscous modulus reveal that smooth muscle is responsible for the aortic wall's viscous behavior.

Roy utilized the term *viscosity* in his examination of arterial tissue to ascribe the material's elasticity "after-action" [172]. This time-dependent phenomenon is evidenced in the tissue's ability to subside vibrations in a rapid manner. While viscosity in metals has been attributed to molecular resistance, it was unknown if the law of molecular friction was applicable in nature. It is well established that smooth muscle cells are the primary cause for viscosity in arteries [31, 71, 174, 210].

Relative Composition in Arterial Tree

Elastin, collagen, and smooth muscle are distinct in their effect on the global arterial biomechanical properties. Accordingly, their relative composition and organized arrangement determine the overall function of healthy tissue. Diseased tissue can be identified by its disproportional quantity and compromised structural integrity of these three constituents. Microstructural composition, and thus biomechanics, determines the tissue's role in the arterial tree.

In the thoracic aortic wall, elastic fibers amount nearly half of dry weight [85]. This value halves near the abdominal aorta [10, 68, 82], which substantiates the unique roles of each region in the same vessel [180]. Collagen-to-elastin (C/E) ratio is an effective parameter associated with vessel stiffness, typically increasing as diameter decreases [49, 68]. The ascending aorta is the most distensible and the carotid artery is the least distensible according to this ratio. The ascending aorta expands to serve as a reservoir during systole, a phenomenon known as the Windkessel effect [24]. The coronary artery, on the other hand, is subjected to repeated external stress from the contracting myocardium and requires increased collagen to withstand these forces [68].

Along the aorta, smooth muscle concentration increases with distance from the aortic valve [10] and performs work to dissipate mechanical energy from the heart muscle [160]. Biomechanical characterization confirms viscous constants are associated with relative amounts of smooth muscle [14, 30, 32]. There is a competitive balance between elastic and viscous moduli along the arterial tree depending on the tissue's role in efficiently transporting blood from the heart.

2.4 Thoracic Aortic Wall Failure

2.4.1 Thoracic Aortic Aneurysm

A thoracic aortic aneurysm, most common in the aortic root or ascending aorta, is an enlargement of the aortic diameter as a result of a weakening wall caused by genetic factors, atherosclerotic disease, or mechanical forces. Smoking, hypertension, and age are risk factors in addition to connective tissue disorders. Marfan syndrome causes cystic medial degeneration, characterized by a

deterioration of elastic fibers, a decrease in smooth muscle cells, and an increase in collagen content. Similarly, Loeys-Dietz syndrome leaves children at risk to aortic aneurysms from connective tissue defects [126]. Aneurysms are associated with decreased elastin and smooth muscle cell content [80] and increased collagen content [89]. As dilation (radius) increases, wall tension increases proportionally according to Laplace's law for a cylindrical vessel. Thus, larger aneurysms grow faster than smaller ones and should be monitored closely to avoid rupture. Thoracic aortic aneurysms are largely asymptomatic, oftentimes only recognized on a routine radiographic examination. In some cases, pseudoaneurysms (false aneurysms) may form in cases when a hematoma develops through the aortic wall without altering the aortic lumen.

2.4.2 Aortic Dissection

Aortic dissections, 65% of which initiate in the ascending aorta, are an acute syndrome where a dissection plane is present in the aortic wall, generating a false lumen [34]. Whether caused by an initial tear in the *intima* or a *vasa vasorum* rupture in the *media*, aortic dissection is an example of intimal failure. Approximately 75% of dissecting aortas experience hypertension [34]. Chronic hypertension increases aortic wall shear stress and initiates intimal thickening adaptations. Conversely, arterial stiffness has been considered a primary cause of hypertension [155] and the pathogenic process is still under debate [141]. However, those with hypertension do not usually experience extensive aortic dilation or suffer aortic dissection, suggesting that hypertension is not the sole cause. As with thoracic aortic aneurysms, genetic disorders must also be considered in the pathogenesis of dissection. Aortic dissection compromises flow to the arteries proximal to the tear and may cause ischemia of the myocardium, kidneys, mesentery, brain, and spinal cord. Aortic dissection may be associated with other complications such as a developing aneurysm or aortic regurgitation, which may be the result of valve insufficiency or false lumen propagating through the aortic root.

2.5 Surgical Interventions

Several procedures have been developed to replace the failed aortic segment with a vascular prosthesis. The following section provides a brief overview of the common surgical treatments of the thoracic aorta.

2.5.1 Aortic Root Reconstruction

Although aortic valve replacement (AVR) will not be discussed in depth, aortic root reconstruction may include replacement of the aortic valve. However, if valve insufficiency (regurgitation) is caused only by root dilatation, the leaflets can be spared and root replaced.

Valve-Sparing Procedures

In cases when the aortic valve is healthy, a replacement graft may be placed in the aortic root position. There are currently two main procedures where this is executed. The *David Procedure* reimplants the native valve with a graft to permanently stabilize the annulus and prevent further aortic dilation. The *Yacoub Procedure*, on the other hand, preserves the natural valve commissures and remodels the graft around the root. This remodeling technique conserves mobility of the annulus. In both cases, coronary buttons are sewn directly into the vascular prosthesis. For a clinical comparison of the two procedures, the reader is directed to [121, 188].

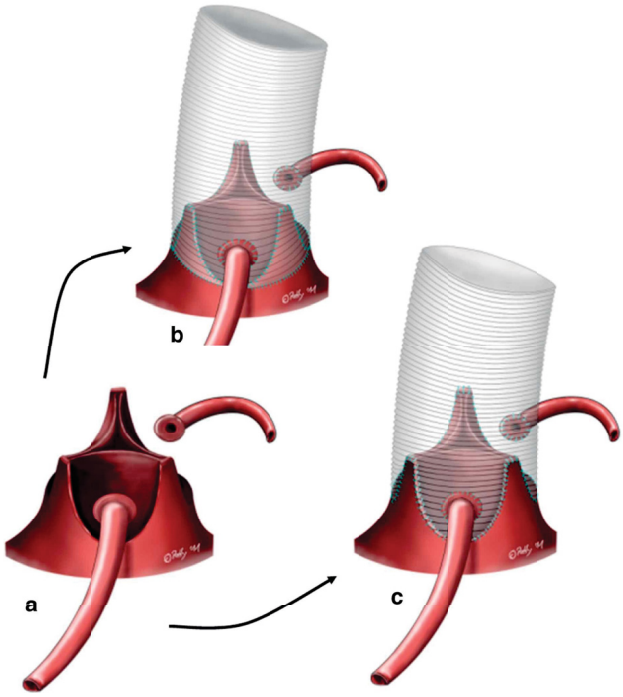

Figure 2.7: Valve-sparing aortic root procedures. **(a)** Isolated aortic valve with coronary buttons. **(b)** David Procedure (Reimplantation). **(c)** Yacoub Procedure (Remodeling). Reproduced from [117] with permission from John Wiley and Sons.

Valve-Replacing Procedure

For compound failure of the aortic valve and root, a composite repair is required. In the case of the modified *Bentall* procedure, a Dacron tube equipped with a prosthetic aortic valve is sewn into the aortic root position [25]. A pulmonary autograft alternative, known as the *Ross* procedure, was introduced in 1967 [171]. The procedure replaces the aortic root with the patient's own pulmonary root. The pulmonary root is then replaced with a cryopreserved cadaver allograft. The motive behind this procedure is to maintain a dynamic, living substitute in the aortic position to foster adaptive mechanisms for withstanding pressure during ventricular ejection. Furthermore, biological valves do not require anticoagulation agents as with mechanical prostheses. The procedure has been criticized for its complexity, which escalates an aortic disease to a potential comorbidity and the

need for reoperation [41,54,116]. Long-term results of the *Ross* procedure support its superior valve hemodynamics to conventional AVR [196], and improved quality of life and survival to homograft replacement [64].

2.5.2 Other Thoracic Aorta Reconstructions

The ascending aorta, aortic arch, and descending thoracic aorta may require reconstruction in the event of an aneurysm or dissection. In a similar fashion to aortic root reconstruction, diseased tissue is resected and replaced with a vascular prosthesis, usually a polyester or polytetrafluoroethylene graft. Thoracic endovascular aortic repair (TEVAR) is a possible non-invasive alternative to correct malperfusion. Although stent grafts are primarily employed in the abdominal aorta, these devices have been utilized in the descending thoracic aorta [4] and recently, the ascending aorta [18, 170].

2.6 Concluding Remarks

Vascular implants replace diseased vessels to restore its primary function: delivering blood to tissue. However, understanding the vascular tissue structure and its mechanical properties are necessary in comprehending its essential biomechanical functions. Arteries display unique heterogeneity associated with its organized structure, manifesting in anisotropy, circumferential compliance, and viscoelasticity. The success of any vascular implant depends on its ability to mimic a dynamic, healthy vessel. Ideally, vascular substitutes should replicate both biological and mechanical characteristics of native tissue. Unfortunately, current vascular prostheses have been found to cause hemodynamic irregularities, biomechanical discontinuities, and vascular complications. In the following chapter, the disparity between native aortic tissue and its replacement, Dacron, will be elucidated.

Chapter 3

Literature Review

This chapter aims to provide the reader a brief overview of the consequences of current vascular prostheses, the state of novel design in ascending aortic grafts, and motivation for the synthetic material presented in this thesis.

3.1 Dacron

The aortic wall is dynamic and living, with a refined set of mechanical properties necessitated by its function. The role of the local aortic wall tissue is determined by its proximity to the aortic valve, the optimal hemodynamics for cardiac efficiency, and current physical demands. An ideal prosthetic material is able to replace all functional properties of native healthy tissue. From a mechanical standpoint, the ideal graft mimics the anisotropy, viscoelasticity, hyperelasticity, and internal residual stresses of the adjacent tissue. Furthermore, the prosthesis must be biocompatible, inert, thromboresistant, and porous [77].

The first clinical use of a porous cloth as an arterial prosthesis was placed in the abdominal aorta of dogs [200]. Blood loss through the cloth mesh was surprisingly minimal. Bleeding ceased after 30 seconds of withstanding arterial pressure. Autopsy revealed that the prostheses were enveloped in scar tissue comprised of fibroblasts and collagen fibers. Fabrics, including Nylon, Teflon, and Dacron, have since been implemented as viable arterial prostheses [56, 83, 162]. Dacron was found to be the most clinically efficient due to its reduced failure incidence and mortality rates. Dacron grafts were shown to sustain long-term patency and maintain sufficient durability [57]. Dacron prostheses are still widely used. However, Dacron graft implantation has caused detrimental effects due to its mechanical disparity with native arterial tissue.

Unlike the aortic wall, Dacron grafts maintain static mechanical properties to provide a conduit for blood. While the graft is successful in restoring flow, its implementation into the aortic column yields sub-optimal functionality in preserving natural hemodynamics, reducing wall stresses, and adapting to current physical demands.

3.1.1 Mechanical Disparities

Dacron grafts exhibit noticeable structural differences from aortic tissue. Dacron grafts are 75% thinner with well-defined corrugations along the longitudinal direction to increase axial distensibility and prevent bending. The aortic wall is comprised of three distinct layers, while Dacron is a woven or knitted fabric. Unsurprisingly, these structural differences yield contrasting mechanical performances. At physiological strain, Dacron is approximately 24 times stiffer than healthy ascending aorta [191]. In accordance with its increased stiffness, Dacron exhibits reduced compliance (circumferential distensibility) [84,108,187,202]. Dacron's exceedingly high circumferential stiffness also results in its increased anisotropy (directional dependency) when compared to healthy ascending aorta [191] and iliac artery [120]. According to Hasegawa and Azuma, both circumferential and longitidunal relaxation strengths match that of the ascending and proximal thoracic aorta [84]. The viscoelastic behavior, or energy-dissipating capacity, of Dacron closely resembles the proximal aorta in this study. This study, however, revealed only normalized stress relaxation values. Circumferential stretch during the stress relaxation tests were 50% and 10% for arteries and grafts, respectively. The different stretch values for these tests makes the comparison ambiguous. Lee et al. determined stress relaxation behavior of arterial tissue and vascular grafts by accounting for equal load, as opposed to strain [120]. Dacron grafts displayed much more relaxation than iliac arteries. It is important to note that elastic and viscous components of a material are not independent of one another, making this assessment unclear. Recent investigation of woven Dacron aims to explain the role of viscoelasticity on *in vivo* dynamics [8, 195]. Understanding of Dacron graft viscoelasticity and its unique effect on hemodynamics is limited and warrants further study.

Dacron grafts expand after initial placement in the thoracic aorta with a distinct early and late growth rate, mimicking a typical creep response of polymers. In the ascending aorta, grafts dilate 17% within a week following implantation, with smaller diameter grafts experiencing higher diameter increase [67]. While the graft seems to adapt to the aorta's geometry and hemodynamic demands through structural changes, its pre-implant circumferential mechanical properties are maintained. This was evidenced in a case study of a woven double-velour Dacron graft explanted after 27 years [147]. Dacron grafts compromise dissimilar mechanical properties for long-term strength and durability. Graft insertion creates discontinuity in the mechanical response of the entire vessel wall, precipitating in abnormal hemodynamics and shear stresses.

3.1.2 Hemodynamic Consequences

To understand the effect of compliance mismatch in the thoracic aorta, it is essential to revisit the concept of Windkessel. The Windkessel effect refers to the ability of large elastic arteries to store blood during systole by distending under high pressure. As blood pressure decreases during diastole, these arteries recoil at a rate determined by its previous distension. In this respect, the aorta itself can be considered a capacitor, which stores and releases energy provided by the heart pump. The capacitance is directly related to the vessel's compliance. This phenomenon is responsible for preserving continuous flow to organs, despite the heart's pulsatility. It reduces

systolic pressure, which effectively decreases left ventricular afterload. It improves coronary flow and myocardial perfusion during diastole [24]. Implementation of an aortic graft diminishes the vessel's capacitance, predictably causing the Windkessel's hemodynamic benefits to decline.

Aortic banding was performed in swine to reduce compliance without introducing an anastomosis or altering the aortic wall geometry. This resulted in an increase of systolic pressure and pulse pressure [99]. Heart rate increased in the two days following operation in order to maintain both cardiac output and normotension. Immediately following a considerable decrease in compliance, characteristic impedance increased dramatically. Characteristic impedance (Z_c), a ratio of forward propagating pressure to flow, is inversely related to the square root of compliance (C):

$$Z_c = \sqrt{\frac{\rho}{A}\frac{1}{C}} \tag{3.1}$$

where c represents wave speed, ρ represents blood density, and A represents the vessel's cross-sectional area. Compliance (C) is the ratio of change in cross-sectional area (A) and change in transmural pressure (p).

$$C = \frac{\delta A}{\delta p} \tag{3.2}$$

However, while compliance recovered slightly in the days following aortic banding, characteristic impedance did not. Pulse wave velocity (c) is related to the characteristic impedance by the following equation:

$$c = \frac{Z_c \cdot A}{\rho} \tag{3.3}$$

$$= \sqrt{\frac{A}{\rho C}} \tag{3.4}$$

Moens-Korteweg formula has estimated this parameter (PWV) with respect to circumferential incremental elastic moduli (E_{inc}), a biomechanical measure of stiffness at an instantaneous strain.

$$PWV = \sqrt{\frac{E_{inc} \cdot h}{2r\rho}} \tag{3.5}$$

where h represents wall thickness, r represents vessel radius, and ρ represents blood density.

As characteristic impedance increases, so does the pulse wave velocity. This, in turn, reduces the return time of waves reflected at the iliac bifurcation and by the periphery, seen in Figure 3.1. Reflected waves arrive at the aortic root earlier. These hemodynamic alterations are revealed in the aortic pressure waves, which exhibit a delayed systolic peak and amplitude increase. The pulse pressure increase is due not only to superposition of the forward and earlier reflected wave, but also due to the individual increase in amplitude of each wave. This study in swine confirmed that the majority of systemic compliance is within the proximal thoracic aorta. This is not surprising given

the role of large elastic arteries in contrast to the rest of the systemic circulation. For this reason, increases on pulse pressure and characteristic impedance become more pronounced when the graft is placed closer to the heart [9, 199].

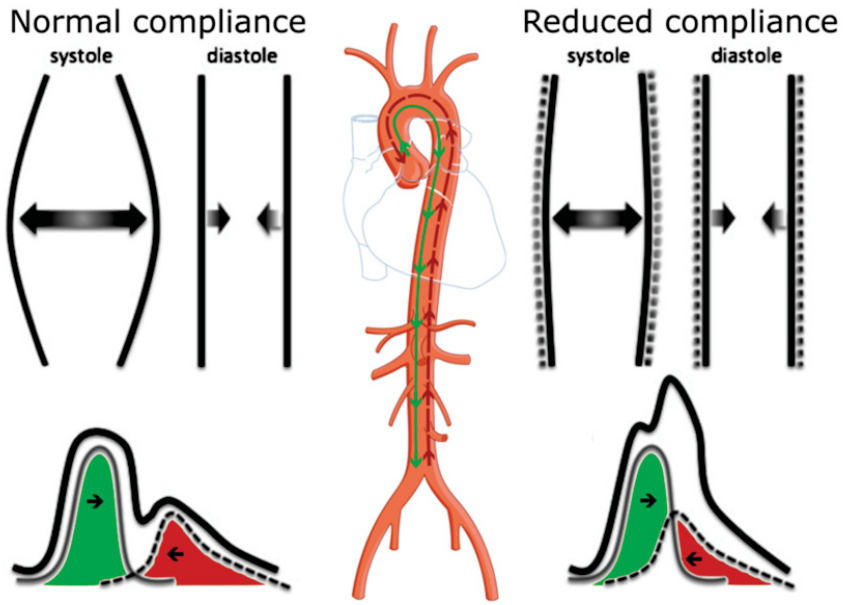

Figure 3.1: Faster reflecting wave results in increased systolic pressure, increased pulse pressure, and decreased diastolic pressure. Adapted from [1] and [104].

The effect of reduced compliance on pulse pressure and characteristic impedance can be witnessed immediately post-operation. Over time, these have deleterious consequences on cardiac pumping efficiency. Specifically, the increase in systolic pressure elevates afterload, the required pressure needed to eject blood [100, 107, 131, 146, 197]. Aortic graft compliance mismatch increases during exercise. Under increased cardiac output, the aorta's Windkessel function is especially vital. Furthermore, patients with grafts experienced much less reduction in peripheral pressure wave reflection during exercise [109]. The left ventricle must overcome a higher input threshold to achieve the same cardiac output, resulting in hypertrophy over time. Left ventricular hypertrophy is a thickening of the left ventricle walls as muscle tissue enlarges. As a result, the left ventricle loses elasticity and may be unable to pump sufficient blood volume to meet body's demands.

Compliance reduction has also been associated to poor coronary perfusion [152, 205]. Roughly 80% of coronary perfusion occurs during diastole [43]. Poiseuille's law states that flow through a cylindrical pipe is proportional to a pressure drop. This premise provided the basis for coronary perfusion pressure (CPP), a quantity describing the pressure gradient between the aortic diastolic pressure and left ventricular end diastolic pressure. Arterial compliance reduction is known to cause an immediate increase in systolic blood pressure, but also sacrifices diastolic pressure over time [93]. This is due to the lack of stored energy within the aorta during diastole. An analysis of the effects caused by increased pulse wave velocity and earlier wave reflections also reveal a decrease in CPP.

In healthy coronary artery hemodynamics, wave reflections decrease the impedance and facilitate flow [218]. Premature wave reflection and higher pulse pressure are linked to coronary artery disease [88, 207]. Surprisingly, *in vivo* subendocardial blood flow increases with a decrease in aortic compliance, despite a decrease in the coronary perfusion pressure. Vascular tone adjusts endocardial blood flow as myocardial oxygen consumption increases. Therefore, an increase in endocardial blood flow does not imply improved coronary perfusion, but rather suggests mild ischemia in the subendocardium [152]. The endocardial/epicardial flow ratio, found to be a more suitable measure of myocardial blood distribution, has been shown to decrease with aortic compliance reduction. Coronary diastolic/systolic flow ratio decreased during increased ventricular contractility. An increase in coronary flow during systole impairs overall coronary perfusion due to the intramyocardial compressive forces [103].

The hemodynamic consequences presented here are a result of reduced compliance, and can also therefore be expected with aging and arterial stiffness. With this in mind, the compliance of a Dacron graft resembles that of a diseased artery at supraphysiological proportions. It induces coronary artery disease, despite the lack of a coronary artery stenosis. Yet, it is considered the gold standard of thoracic aorta reconstruction. One can expect these effects to become pronounced with proximity to the heart and quantity implanted. Beyond the hemodynamics, the Dacron graft prosthesis has detrimental effects on the surrounding wall tissue.

3.1.3 Anastomoses

Compliance mismatch and wall thickness discontinuity at the anastomosis generates flow disturbances and abnormal stress concentrations. Mathematical models of synthetic graft implantation, not accounting for remodeling, calculate circumferential stress concentrations at the suture line, contributing to possible anastomotic rupture [19, 37, 156]. The suture-line is a site of injury, and remodelling is to be expected as a result of the healing process [7]. Intimal thickening occurs when vascular smooth muscle cells proliferate in the *intima* layer, reducing lumen area and introducing flow disturbances. The influence of Dacron graft implantation on subsequent intimal hyperplasia is still under question. In end-to-end anastomosis of dog femoral arteries, intimal thickening developed, despite both ends holding similar compliance [101]. Flow patterns revealed that intimal thickening is determined by local wall shear stresses [114, 145], and initiates near the point of flow separation [101]. Intimal thickening has also been observed near moderate stenoses, where flow separation occurs despite the absence of an anastomotic joint [22]. Still, analysis of end-to-side anastomosis in dogs revealed a larger increase in maximal intimal thickness at the suture line when using a polytetraflouroethylene (PTFE) graft than when using a more compliant vein graft [23]. This seems to suggest that the vascular healing response may correspond to compliance mismatch. However, the hemodynamic variability between end-to-side and end-to-end geometries limit their comparability. In an end-to-end anastomotic model, the effect of compliance mismatch was investigated in the common iliac artery of dogs by banding to preserve vessel geometry. The compliance mismatch exposed negligible effect on intimal thickening in banded and control vessels. Graft

anastomosis in the femoral artery induced near-occlusive neointimal hyperplasia [154]. Therefore, compliance mismatch is not solely responsible for intimal thickening, at least in end-to-end anastomoses. It seems that the use of sutures is required to induce significant intimal hyperplasia. A similar experiment was conducted with external Dacron meshes of autologous venous grafts used in femoropopliteal reconstruction (end-to-side) in sheep. Compliance mismatch introduced intimal hyperplasia in the distal anastomosis [193]. Flow measurements identified regions of flow reversal did not necessarily correlate with intimal hyperplasia in those regions, but with the overall incidence of intimal hyperplasia. When comparing between graft-artery anastomoses types, graft compliance holds significant influence on maximum stress concentrations only in end-to-side anastomoses [19]. In end-to-end anastomoses, flow separation and corresponding low wall shear stresses are prominent factors in intimal thickening.

The wall shear rate distribution in an end-to-end anastomosis model was determined to investigate the role of hemodynamics in the development of intimal hyperplasia. In a diameter mismatch, shear rate elevates at the proximal anastomosis of the smaller graft and diminishes to nearly zero at the distal anastomosis. In a compliance mismatch, shear rates also decrease at the distal anastomosis [167]. Intimal hyperplasia initiates in regions of flow separation and recirculation zones, which occur at the distal anastomosis [185]. This work suggests that compliance mismatch is a factor in intimal thickening due to its geometric effect on wall shear rate, rather than its mechanical disparity. Nonetheless, it is imperative that vascular grafts match both compliance and diameter to limit flow disturbances.

3.1.4 Long-Term Failure

Compliance mismatch also plays a role in long-term patency and viability *in vivo*. Reduced compliance has been related to diminished vascular patency over time, even with optimal flow surfaces [3, 165]. In addition to intimal thickening, thrombosis and endothelial cell damage can transpire through platelet interactions with the prosthesis [29, 81]. Stress concentrations, caused by compliance mismatch, may induce anastomotic pseudoaneurysms through progressive damage of the adjacent wall [136, 190]. Efforts have been made to minimize the anastomotic compliance mismatch by adjusting suture materials and surgical techniques [189]. However, improving flexibility at the anastomosis does not rectify the inherent microstructural and biomechanical differences between graft and artery. Decreased graft compliance is not always compensated by increased durability. While mechanically capable to withstand forces of the vascular wall, grafts may still fail at the suture line where stresses are highest. Coincidentally, increasing graft compliance will decrease these anastomotic stress concentrations.

Suture line mismatch is not the only mechanism by which large-diameter grafts fail. Grafts can experience uncontrolled dilatation and fiber deterioration [28, 161]. Individual fibers within the textile graft experience creep over time, reducing their initial resistance to tension. In some cases, pseudoaneurysms and non-anastomotic rupture of the Dacron graft can occur [105, 106, 214]. Fatigue failure, while seldom, is often unpredictable [52].

3.2 Novel Vascular Graft Design

When compared to aortic vascular grafts, the significant decrease in patency of small-diameter synthetic grafts (<6 mm diameter) [3] have motivated the search for more suitable options [77]. Current vascular grafts are biocompatible and resistant to fatigue, but mechanical properties of polyethylene terephthalate (PET) or expanded polytetrafluoroethylene (ePTFE) differ vastly from those of healthy arteries. Although viable in large-diameter vessels, the mechanical disparity is pronounced in small-diameter vessels. New tissue engineering strategies and compliant polymers have been considered to correct this major drawback.

3.2.1 Tissue Engineering

A perfect vascular graft replaces a diseased vessel with a biologically and mechanically healthy vessel. Due to the low patency rate of small-diameter synthetic grafts, the gold-standard replacement in coronary or peripheral bypass surgeries are autologous grafts. A tissue-engineered vascular graft (TEVG) aims to reproduce autologous grafts through the use of biodegradable scaffolds seeded with vascular cells. For this reason, TEVGs are sometimes considered tissue-engineered blood vessels (TEBVs). Unlike current vascular grafts, TEVGs are expected to remodel *in vivo* so that they become biologically, mechanically, and hemodynamically invisible to adjacent tissue [157].

In 1986, Weinberg et al. used a Dacron mesh as a platform to seed bovine endothelial cells, fibroblasts, and smooth muscle cells on a collagen matrix [208]. Since then, novel polymers have been utilized as mechanically stable scaffolds to mimic the complex multi-layered arterial structure. Hibino et al. developed a biodegradable composite scaffold of polyglycolic acid (PGA), poly-ε-caprolactone (PCL), and poly-L-lactide (PLLA) to demonstrate long-term patency [92]. Autologous bone marrow-mononuclear cells aspirated from the anterosuperior iliac spine were seeded onto the composite scaffold and implanted as extracardiac cavopulmonary conduits for young patients with single ventricle physiology. Regenerative and adaptive TEVGs maintain strong appeal in treating congenital heart disease in patients with young, maturing, low-pressure vessels. In this first human trial, some grafts experienced stenosis, but were rectified following percutaneous angioplasty. Histopathologic examination at midterm follow-up revealed endothelialization and scaffold degradation [179]. Long-term follow-up revealed patency at 6 years, with 40% of patients not receiving any anticoagulant medication. While this study demonstrates long-term feasibility of TEVGs in humans, these results cannot be translated to vessels under high pressure. The slow tissue formation rate lags behind scaffold degradation and results in loss of mechanical support over time.

Preconditioning TEVGs using mechanical stimulation *in vitro* from bioreactors have been considered to accustom both the synthetic scaffold and seeded cells to physiologically relevant stresses [150]. In the right saphenous artery of Yucatan miniature swine, autologous grafts that underwent mechanical stimulation remained patent for 4 weeks, while those prepared under static conditions developed thrombosis after 3 weeks [149]. In an effort to limit TEVG manufacturing

time, TEVGs can be prepared by decellularizing a biodegradable PGA scaffold previously seeded with smooth muscle cells and extracellular matrix proteins [163]. The decellularization process preserves vessel geometry, biological structure, and mechanical stability, while limiting immunogenicity introduced by foreign cells. These decellularized TEVGs showed patency rates above 80% as murine aortic interposition grafts [163], porcine carotid artery grafts [164], canine coronary artery bypass conduits, and baboon arteriovenous fistulas [51]. These TEVGs displayed significant remodeling to match the tissue structure of adjacent vessels. Anastomotic intimal hyperplasia was dramatically lower as compared to current vascular grafts. Explanted TEVG segments did not experience any loss in suture strength, burst pressure, or compliance. Biodegradable PGA scaffolds coated with poly-4-hydroxybutyrate were seeded with myofibroblasts and implanted in the main pulmonary artery of growing lambs [94]. The implanted TEVGs grew in diameter and length as animals increased body weight. Biodegradable polymers are reasonable scaffold materials in developing TEVGs that can adapt over time. This ability to remodel separates TEVGs from current grafts, which aim to remain inert and sustain their mechanical properties. Even so, polymeric scaffolds are not necessary to produce a biological vascular graft.

L'Heureux et al. demonstrated that a complete human blood vessel can be formed *in vitro* [122–124]. These vessels are completely biological and hold burst pressure of the internal mammary artery and match compliance of the human saphenous vein. Other methods of producing completely biological, but acellular, vascular conduits have also been developed. Boland et al. formed vascular scaffolds by electrospinning collagen and elastin [33]. Multiple layers of different collagen/elastin compositions attempt to replicate the physiological, three-dimensional protein distribution of the extracellular matrix.

3.2.2 Synthetic Polymers

Synthetic scaffolds alone have also been reviewed as a viable option. Cell harvesting introduces infection risk and can be a limiting factor for patients without sufficient cell volume. Furthermore, the time required to culture cells necessary for seeding prevents its ready availability, even for decellularized scaffolds. A small-diameter tubular scaffold composed of PGA knitted fibers, PLLA/PCL sponge, and PGA/PCL reinforcement was implanted in the canine inferior vena cava [134] and pulmonary artery [133] for 12 months. In both cases, there was no stenosis nor thrombosis. There was no significant difference in elastin content between the graft and native vessel. A similar graft compounded with collagen was implanted in the carotid artery of dogs [215]. Incorporating collagen increased the number of adhered cells *in vivo* and promoted tissue infiltration. After 12 months *in vivo*, the graft exhibited similar tensile modulus, tensile strength, and collagen content of the native artery.

There has been investigation in other synthetic polymers that offer more compliance than current grafts composed of PET or ePTFE. Tai et al. developed compliant poly(carbonate)polyurethane (CPU) grafts by cast coagulation on a rotating steel mandrel [187]. Under a pulsatile flow circuit, when compared to Dacron and ePTFE, the CPU vascular graft exhibited a closer compliance and

stiffness to human muscular artery. Compliance mismatch increased at higher physiological pressures, for which the CPU graft was not intended. The use of particular polymers or manufacturing processes cannot be easily translated across various diameters and pressures. For example, electrospun nanofibrous PLLA grafts were too stiff compared to ovine femoral [17] and human carotid and femoral arteries [6].

It can be difficult to find a synthetic polymer that exhibits the arterial viscoelastic characteristics. Lee et al. constructed polyurethane grafts by aligning fibers at various angles [120]. Relaxation rates of these grafts relied heavily on the fiber orientation. A similar graft was also found to be more viscous than canine carotid arteries, but resembled closely the frequency-dependent viscosity of femoral arteries [96].

The low rate of large-diameter graft-related complications have prioritized the innovation of novel and compliant grafts for small-diameter vessels. However, the compliance mismatch in large-diameter vessels necessitates similar breakthroughs. There have been very few advances in large-diameter vascular grafts. De Paulis et al. adapted a woven Dacron graft to incorporate a three-layer structure to improve blood impermeability [58]. However, introducing an outer layer of ePTFE resulted in an even stiffer graft. New polymers must also be considered for large-diameter vascular grafts where patency should not be the sole concern. Compliance mismatch at high pressures lead to consequences downstream of the systemic circulation.

3.3 Poly(vinyl Alcohol)

Poly(vinyl alcohol) (PVA) is a biocompatible polymer of interest in biomedical applications due to its ability to reproduce the hyperelastic stress-strain response observed in most biological tissues. Much research has been conducted to explore production methods to modify its mechanical behavior for particular applications. The mechanical versatility and ease of manufacturing of this polymer make it a viable candidate in investigating new vascular prosthetic materials.

3.3.1 Cryogel Preparation

When crosslinked, PVA can form a hydrogel of desired geometry and mechanical properties. Crosslinking can be induced chemically *via* toxic agents like formaldehyde and glutaraldehyde [97]. Alternatively, PVA can be chemically crosslinked through radiation or electron beam to avoid toxicity and bioactivity within the resulting matrix [132]. The third preparation method generates crosslinks through crystallite formation. These physical crosslinks exhibit higher mechanical strength than chemical crosslinks due to the crystallites' three-dimensional structure [86]. Aqueous PVA solutions can achieve crystallite formation through heat treatment. The first use of freeze-thaw cycles to form PVA hydrogels was reported in 1975 [159]. Hydrogels prepared through repeated cycles of freezing and thawing are termed *cryogels*.

In the pioneering study by Peppas, crystallite formation correlated with initial PVA concentration, freezing time, and thawing time [159]. Since then, many efforts have been made to understand

crystallite formation and characterize these gels according to various processing parameters. PVA, seen in Figure 3.2a, contains a hydroxyl group that permits hydrogen bonding when dissolved in water. Thermal cycling induces phase transitions which generate and restructure crystalline domains along the polymer chains. When the aqueous solution is frozen, water freezes and creates regions of high polymer concentration, shown in Figure 3.2b. Crystallites form in these regions, while pores form in areas of low polymer concentration [216]. Upon thawing, a PVA cryogel (PVA-C) is formed. Each instance of freezing and thawing constitutes a freeze-thaw cycle (FTC). Repeated FTCs reorganize the amorphous polymer matrix during crystallization. Conditions of the FTCs determine the final polymer structure. Some of these conditions include the freezing and thawing temperatures, holding times at these temperatures, freezing and thawing rates, and the number of cycles [203]. As these cryogels closely mimic the mechanical behavior of biological tissues, the effect of these processing parameters on non-linear elasticity and tensile strength are particularly relevant. Using a modified Mooney-Rivlin strain energy function, Pazos et al. correlated cryogenic treatment parameters to material model coefficients [158].

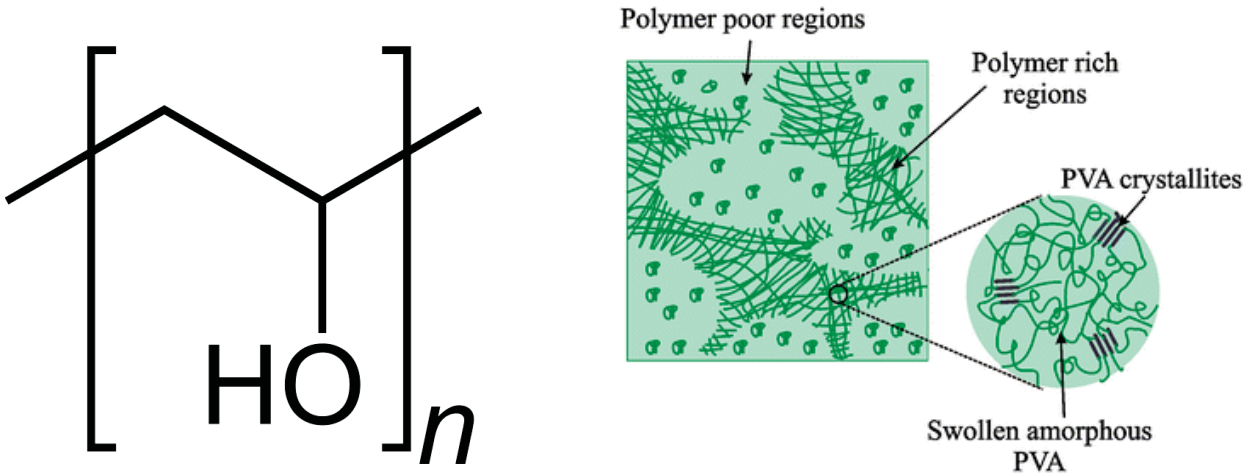

(a) (b)

Figure 3.2: **(a)** Hydroxyl group $[OH^-]$ in PVA facilitates hydrogen bonding. **(b)** PVA crystallites form in polymer rich regions and pores form in polymer poor regions. Reproduced from [59] with permission from Springer Nature.

PVA Concentration

Higher concentrations produce gels with higher levels of crystallinity due to the increased presence of hydroxyl groups. Cryogels produced with higher concentrations had lower degrees of swelling, suggesting decreased porosity and increased crosslinking [87, 192]. The formation of crosslinks provides rigidity to the cryogel, which derives from an aqueous solution. The increase in crosslinks, therefore, should improve cryogel stability. Increases in PVA concentration result in reduced compliance and increased cryogel elastic modulus [127, 204].

Viscoelasticity in polymers is associated wtih resistance to chain rearrangement. Under com-

pression, stress relaxation rate and creep increases with increasing polymer concentration [204]. The amount of stress relaxation increases with decreasing polymer concentration [111]. The effect of PVA concentration on the cryogel's viscosity is difficult to assess since polymer concentration also affects its elasticity.

Freezing and Thawing Temperatures

During freezing, PVA solutions reach a supercooling temperature, at which crystallization begins to occur. Due to the phase transition that occurs, temperature in the solution increases from the latent heat of crystallization [128]. In a 10% PVA solution, supercooling temperature is around -8°C, but decreases even further with increasing PVA concentration [128, 158]. Lozinsky et al. showed that freezing temperature alters the ratio of frozen and unfrozen solvent [127]. Higher freezing temperatures permit chain mobility due to the increase in unfrozen solvent. When held frozen for 10 days, PVA cryogels formed at -10°C are more rigid than those held at lower temperatures [129]. However, for reliable freezing below the supercooling temperature, most protocols opt for freezing temperatures below -10°C. During thawing, ice melts around 0°C, resulting in slight delay in temperature increase of the PVA solution [62]. While PVA cryogels can be thawed to room temperature, Pazos et al. determined that there was no significant difference between a thawing temperature of 10°C and 20°C [158]. Ice acts as a porogen, leaving pores once melted [127]. Therefore, a thawing temperature sufficiently above 0°C will ensure complete melting.

Holding Times

Mechanical strength of PVA cryogels is related to the amount of time spent in freezing temperatures, up to a certain threshold [127]. Holding PVA solutions at -20°C at 1 or 6 hours showed negligible difference in tensile stress and elastic modulus of the resulting cryogel [203]. Holding time in thawing temperatures holds less relevance since crystalline domains develop only at freezing temperatures.

Freezing and Thawing Rates

It is possible to form PVA cryogels through repeated transfers between room temperature and freezing temperature [183]. However, the rate at which FTCs occur can be controlled to generate reproducible properties. It is expected that slower rates would allow polymer chains to rearrange and produce structures of high organization and mechanical stability. Lozinsky et al. confirmed that slower thawing rates increased both crystal size and number [127,130]. Analysis of mechanical properties reveal a greater dependence on thawing rate over freezing rate [144,158,203]. This is due to the increased mobility of polymer chains during the thawing phase, specifically because of the prolonged time in the temperature region from -5°C to -1°C [62,127,129]. For this reason, thawing rate is most important in controlling elastic properties [129, 158].

Number of Cycles

There is a benefit to preparing PVA cryogels through repeated FTCs, as opposed to a single FTC of comparable time. Considering the high efficiency of gel formation during thawing, greater crystalline formation occurs with additional thawing phases [183]. As expected, increasing the number of FTCs amplifies stiffness by supplementing crystals with each FTC [87, 144]. There is, however, an upper threshold to the number of FTCs, by which the elastic modulus no longer increases [158, 216]. Possible polymer chain rearrangements diminish and PVA-C pore size reduces to a certain point. Up to this point, it may be beneficial to increase the number of FTCs instead of reducing thawing rate in order to minimize processing time while achieving similar mechanical properties [158].

3.3.2 Cardiovascular Applications

PVA cryogels have been considered for several biomedical applications, including a surgical embolic sponge [186]. Its compressive mechanical properties have been compared to those of intervertebral discs [204] and articular cartilage [111, 112, 182]. PVA cryogels have been employed as arterial phantoms for magnetic resonance imaging [45] and ultrasound methods [69, 110]. These cryogels have also been considered for aortic prostheses.

Aortic Valve

Jiang et al. designed a tri-leaflet valve with stent and sewing ring using PVA-C [102]. Leaflet geometries determined by the cavity mold were effectively reproduced in the resulting PVA-C, illustrating its accurate and versatile manufacturability. Under cyclic flow, the PVA-C heart valve expanded circumferentially, which is essential in reducing stress concentration at the commissures. This particular design has the potential to compress into a small opening in the chest cavity, avoiding the need for open heart surgery. Bacterial cellulose (BC) is a nanomaterial that can be paired with PVA to mimic the composite behavior of collagen and elastin, respectively [138]. Mohammadi et al. utilized a PVA-BC nanocomposite to create a valve that mimics the mechanical properties of the porcine aortic heart valve [142]. Anisotropy was achieved by applying strain throughout the FTCs to offset crystal reinforcement [139]. Additional refinement is necessary to match the degree of anisotropy present in the aortic valve. Elastic moduli was characterized by uniaxial testing in both principal directions, but the study requires more investigation into the composite's behavior under pulsatile conditions.

Aorta

Bioprosthetic heart valves need a compliant aortic root for optimal hemodynamics. Wan et al. developed a PVA-C stent prototype for bioprosthetic heart valves [203]. The cavity mold design included rings for stent suturing. Their PVA formulation mimicked the anisotropic nonlinear stress response of the porcine aortic root, ensuring the prosthesis and aortic root expand at

the same rate [139]. Stress relaxation tests reveal the PVA-C does not match the initial or final relaxation rates of the porcine aortic root. Dynamic viscoelasticity of PVA-C resembled that of a dog aorta and can be easily modified by changing the initial PVA concentration [115].

Chemically cross-linked PVA has been shown to be nontoxic, compliant, and patent in the infrarenal aorta of rats [40]. Tubular PVA-C was a viable abdominal aorta replacement in rats [48]. However, when PVA-C was treated with a decellularized vascular matrix, thrombi formed and animals died 3-4 days after surgery. Hemocompatibility is an issue with PVA-C and several methods have been utilized to improve blood-material interaction [5]. Covalent attachment of fibronectin not only improves cell attachment, but dramatically enhances cell proliferation [140, 151, 217]. Coating PVA-C with collagen also improves initial attachment and proliferation of bovine aortic vascular smooth muscle and endothelial cells [201].

Chapter 4

Materials and Methods

This chapter presents an overview of the materials and methods used to conduct the experiments and analysis. Viscoelastic theory and characterization is introduced.

4.1 Formation of PVA Cryogels

PVA solutions were prepared by mixing fully hydrolyzed PVA powder (P1763, Sigma-Aldrich, St. Louis, MO, USA) in deionized ultra-filtered water. PVA solutions were mixed at 10%, 15% and 20% (w/w). The solution is stirred at 90°C until dissolution. Once cooled to room temperature, the solution is poured into an aluminum mold and set for 2 hours to eliminate bubbles. A temperature probe was placed inside the solution within the aluminum mold to monitor temperature during cycling. The aluminum mold is set on a programmable chilling/heating plate (EchoTherm™ IC25XT, Torrey Pines Scientific, Carlsbad, CA, USA) placed inside a freezer. The chilling/heating plate was insulated by styrofoam. A custom-made program in LabVIEW (National Instruments, Austin, TX, USA) controlled the programmable plate during freeze-thaw cycles.

A freeze-thaw cycle consisted of:

- $\frac{1}{3}\frac{^{\circ}C}{min}$ freezing rate
- $-20^{\circ}C$ for 1 hour
- $\frac{1}{9}\frac{^{\circ}C}{min}$ thawing rate
- $10^{\circ}C$ for 30 minutes

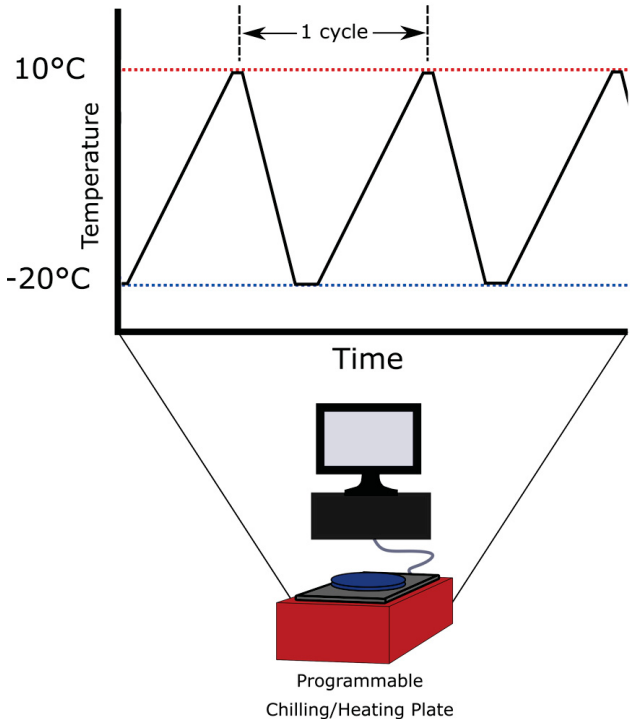

Figure 4.1: PVA cryogel in aluminum mold undergoing freeze-thaw cycling process.

Following completion of freeze-thaw cycles, formed PVA-C was immersed in water and refrigerated until testing. Unless otherwise noted, all tested PVA-C samples underwent 12 FTCs.

4.2 Tissue Collection and Preparation

4.2.1 Tissue Collection

Human ascending aortic tissue ($n = 16$) were obtained following aortic reconstruction surgeries at Montreal Heart Institute and tested within 24 hours. *Healthy* samples ($n = 6$, age 43.8 $\pm$ 7.6 years, 6/6 male) received from excised aortic root during *Ross* procedures. *Aneurysmal* samples ($n = 10$, age 54.0 $\pm$ 14.2 years, 8/10 male) received from excised aortic root or ascending aorta during *Yacoub* or *Bentall* procedures. Samples were refrigerated in media solution until testing. Excess connective tissue in the intimal layer was removed. Circumferential direction of the tissue was marked with red tissue dye before trimming tissues into testing samples. Tissue preparation is shown in Figure 4.2.

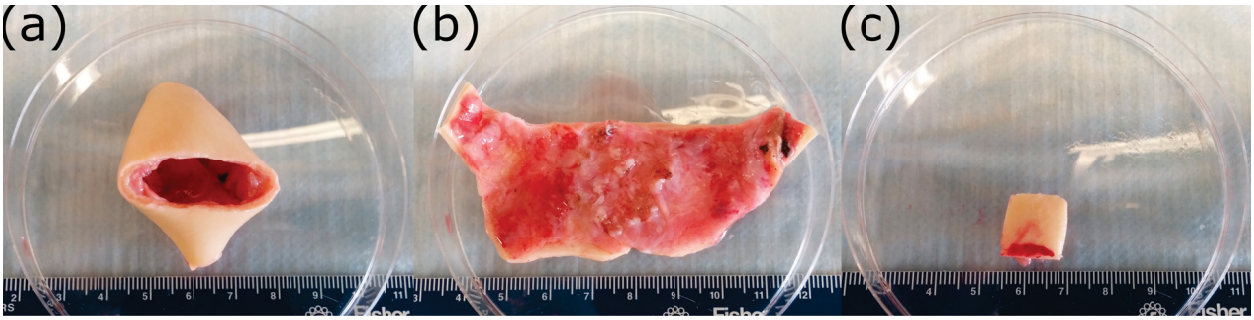

Figure 4.2: **(a)** Excised aortic ring in the residual stress configuration. **(b)** Aortic tissue in a zero-stress state. **(c)** Final trimmed sample with circumferential direction labeled. Scale in cm.

4.2.2 Histology

A small piece of aortic tissue adjacent to each testing square was preserved in 10% (v/v) buffered formalin. The tissue was paraffin embedded, and 5-10 μm thick sections were prepared and stained with Movat's pentachrome to assess vessel elastin, collagen, and smooth muscle cell content. Five 20×-magnified images were obtained for each section representing the media. Images were captured with a QICAM color video camera interfaced with a microscope (CKX41, Olympus Corp., Tokyo, Japan). Percent micrograph field coverage of medial elastin, collagen, and smooth muscle was quantified for each image using ImageJ (Version 1.52a). Color thresholds were adjusted to identify pixels depicting elastin (black/violet), collagen (yellow), and smooth muscle (red). A single data point per patient represents an average histologic quantification of five regions of inquiry around the aortic circumference.

4.3 Mechanical Testing

In vitro planar biaxial tensile testing has been widely used to characterize arterial tissue [13, 16, 60, 66, 74, 143, 153]. Biaxial tensile testing identifies the tensile behavior of a material in two distinct directions under physiological multi-loading conditions. This reproducible testing method provides understanding of local tissue's hyperelasticity, anisotropy, and viscoelasticity.

4.3.1 Biaxial Tensile Test

PVA cryogels, aortic tissue, and commercially available Dacron grafts (Hemashield Platinum, Woven Double Velour Vascular Graft, MAQUET Cardiovascular LLC, Wayne, NJ, USA) were cut into 15×15 mm^2 samples. Thickness measurements were performed along the sample in quintuplicate with a digital thickness caliper (Litematic VL-50A, Mitutoyo Corp., Japan). The sample is assumed to hold constant thickness at the average value for subsequent analysis. Dacron grafts were considered to have 0.35 mm thickness. All samples were fastened with 4-0 prolene sutures to mount on the tensile arms. The no-load length was measured between sutures by a caliper. The sample was loaded in the ElectroForce Planar Biaxial TestBench (TA Instruments, New Castle,

DE, USA), seen in Figure 4.3, equipped with WinTest software (V8.0, Build 2011). All samples were immersed in buffered solution at 37°C for 15 minutes prior to testing to attain thermal equilibrium and subsequently throughout all testing. Samples were preloaded to a force of 0.05 N in both directions before testing to ensure sutures were slightly tensioned. Samples underwent 10 preconditioning cycles loading and unloading at a strain rate of 0.4 mm/s to a displacement of 6 mm in both directions. Depending on suture location, this corresponds to a maximum strain of 60-65%. Following preconditioning, 7 experimental cycles were performed at a strain rate of 0.1 mm/s at the same displacement. Immediately following the last experimental cycle, the sample was pulled to 6 mm displacement at a rise time of 1 second. The sample was held at this displacement for 2000 seconds and stress relaxation response recorded. The sample was slowly unloaded at 0.1 mm/s to its starting position and quickly loaded in a similar fashion for a total of 5 cycles.

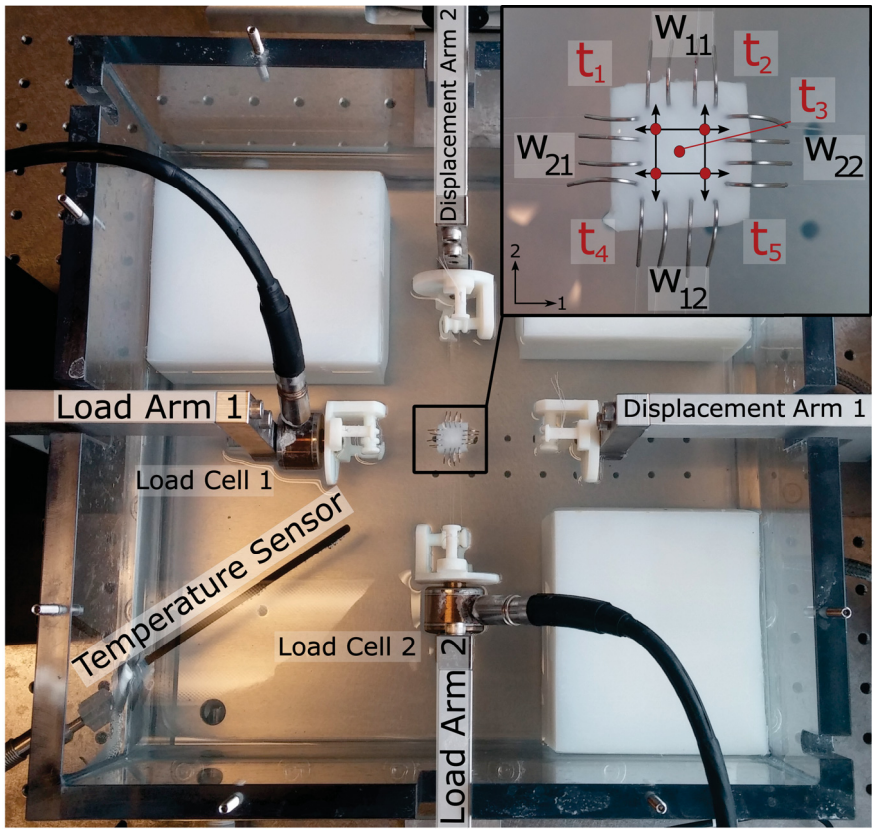

Figure 4.3: ElectroForce Planar Biaxial TestBench setup loaded with PVA sample. Inset displays suture layout of the sample, including locations of thickness measurements (t) and definition of gauge lengths (w) between sutures.

4.3.2 Dynamic Mechanical Analysis

Dynamic mechanical analysis (DMA) assesses a material's viscoelastic properties at different frequencies. Unlike standard biaxial testing at a single strain rate, DMA collects data across a frequency sweep. This provides detail into the material's frequency dependence as well as its

response across physiological frequencies.

In a similar fashion, PVA cryogels, aortic tissue, and Dacron fabric were measured and loaded into the test set-up, seen in Figure 4.3. Sample dimensions were input into the WinTest DMA software (V7.1) to internally calculate strain for testing. All DMA tests were performed uniaxially. Samples were preloaded to a force of 0.05 N in the circumferential direction. The sample was then loaded to 35% mean strain at 0.5 mm/s and held for 10 seconds. Step-sine excitation was performed from 0.1-20 Hz with a dynamic amplitude of ±25%. Frequency oscillations occurred at 0.5 Hz increments. Before each harmonic excitation, the 35% mean strain was maintained for 10 seconds. Complex modulus and phase delay were collected following a preconditioning period of 10 seconds, which commences after oscillations reach full amplitude (10% to 60%). The sample was unloaded after all frequency conditions were completed.

4.4 Analysis

4.4.1 Stress-Strain Curves

The stress-strain response is assigned quantitative parameters to describe mechanical behavior of the material. Various stress and strain definitions have been used to characterize tensile properties.

Engineering Stress and Strain

Engineering stress (σ^{eng}) is defined as the force (F) divided by the initial (no-load) cross-sectional area (A_0).

$$\sigma^{eng} = \frac{F}{A_0} \tag{4.1}$$

where $A_0 = w_0 t_0$ and w and t are width and thickness, respectively, of the sample. Width is measured along the direction normal to the force direction.

Engineering strain (ε^{eng}) is defined as the change in length divided by the initial (gauge) length (w_0). Change in length is determined by the displacement arms. Length is measured along the force direction.

$$\varepsilon^{eng} = \frac{w - w_0}{w_0} \tag{4.2}$$

Cauchy Stress and Strain

Engineering stress and strain measures force with reference to the initial configuration. During tensile testing, initial cross-sectional area is altered. Cauchy stress and strain definitions are defined in the deformed configuration, as opposed to the initial configuration. These definitions are more pertinent in characterizing material's undergoing large strains and increased deformation. Assuming an incompressible ($J = 1$) material, volume must remain constant. This yields:

$$\sigma = \frac{F}{A} = \sigma^{eng}\left(1 + \varepsilon^{eng}\right) \tag{4.3}$$

$$\varepsilon = \ln\left(\frac{w}{w_0}\right) = \ln\left(1 + \varepsilon^{eng}\right) \tag{4.4}$$

Incremental Elastic Modulus

In nonlinear materials, elastic modulus is a function of the strain. Hyperelastic material models, such as Mooney-Rivlin, Ogden, and Yeoh model have been utilized to classify biological tissue with material constants. For simplicity, measuring elastic modulus at different strains can provide information of the overall hyperelastic behavior. Incremental elastic modulus is defined as the instantaneous slope at a strain value. Employing polynomial functions in MATLAB, incremental elastic modulus of Cauchy stress values was calculated at low (15%) and high (45%) engineering strain values.

4.4.2 Energy Loss

Energy loss is a viscoelastic parameter derived from the equibiaxial loading-unloading results. It is an effective measure of the material's ability to dissipate energy. During unloading, the material does not release the same amount of energy as it absorbed during loading. This dissipation of energy into the material results in a hysteresis loop. Energy loss quantifies the energy dissipation capacity of a material using the proportional area of the hysteresis loop. Energy loss is the percentage of strain energy dissipated by the material during unloading from the total energy absorbed by the material during loading. Energy loss is the area of dissipated energy over the area under the loading curve. The area under the stress-strain curve is a strain energy per unit volume and the ratio of both areas yields a unitless quantity. The ratio is presented as a percentage.

$$W_L = \int_0^{\varepsilon_{max}} \sigma_L d\varepsilon \tag{4.5}$$

$$W_U = \int_0^{\varepsilon_{max}} \sigma_U d\varepsilon \tag{4.6}$$

$$Energy\ Loss = \frac{\displaystyle\int_0^{\varepsilon_{max}} \sigma_L d\varepsilon - \int_0^{\varepsilon_{max}} \sigma_U d\varepsilon}{\displaystyle\int_0^{\varepsilon_{max}} \sigma_L d\varepsilon} \tag{4.7}$$

$$Energy\ Loss = \frac{W_L - W_U}{W_L} \tag{4.8}$$

where W_L and W_U refer to the energy absorbed during loading and energy released during unloading, respectively.

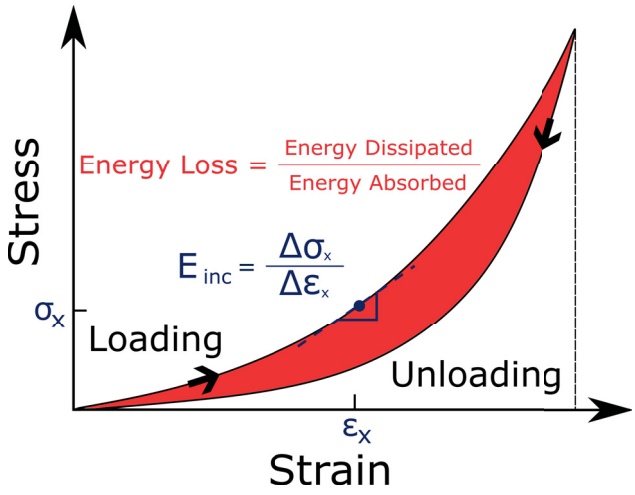

Figure 4.4: A typical hyperelastic stress-strain response displaying hysteresis. Graphical representation of energy loss and incremental elastic modulus is depicted.

4.4.3 Stress Relaxation

Linear viscoelastic models estimate the time-dependent behavior of materials with a linear stress-strain relationship. These materials can be modeled by combinations of springs and dashpots to represent elastic and viscous components, respectively. Constitutive models using these mechanical elements are shown in Figure 4.5 below.

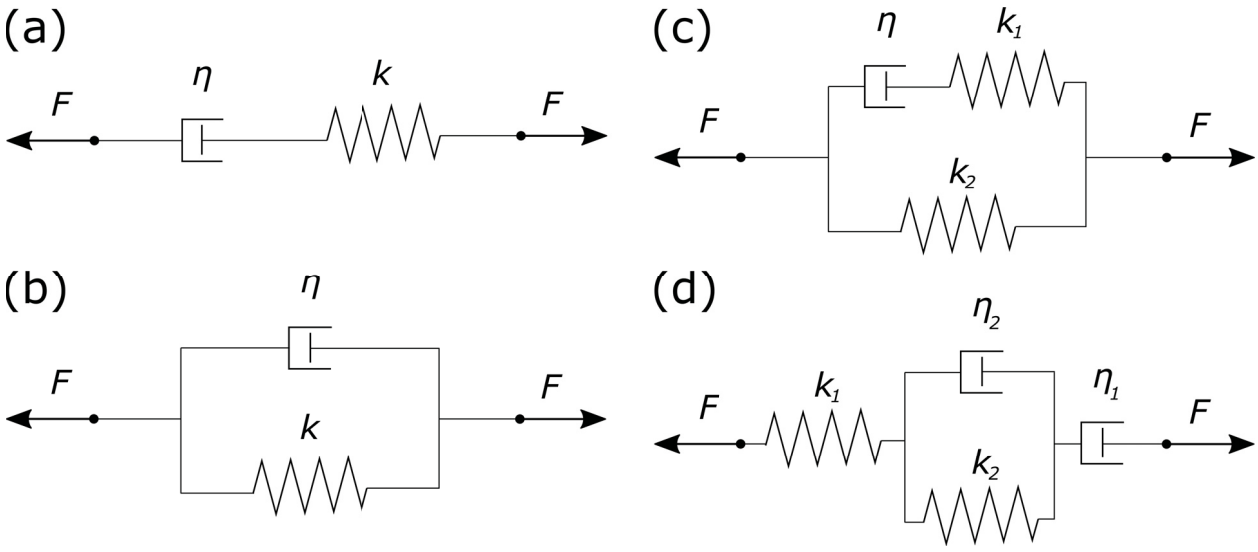

Figure 4.5: **(a)** Maxwell model. **(b)** Kelvin-Voigt model. **(c)** Standard linear solid model. **(d)** Burgers model.

These elements hold constitutive equations to describe their individual behavior. A spring is linear elastic, obeying Hooke's law in Equation 4.9, where k is the stiffness.

$$\sigma = k\varepsilon \tag{4.9}$$

Stress response of the viscous dashpot, shown in Equation 4.10, depends on the rate of strain, rather than the strain itself. The parameter η refers to the material's viscosity.

$$\sigma = \eta\dot{\varepsilon} \tag{4.10}$$

The arrangement of mechanical elements determines how force and displacement are acting on each individual element in relation to one another. These models yield one or more exponential decays to describe stress relaxation. For large deformations, linear viscoelastic models are insufficient to describe the nonlinear stress-strain behavior of biological tissue.

Quasi-linear Viscoelasticity

Fung developed a constitutive equation to describe the nonlinear stress-strain and viscoelastic behaviors [70,71]. Stress is calculated through a linear convolution integral of a reduced relaxation function, $G(t)$, and an instantaneous elastic stress response, $\sigma^e(\varepsilon)$.

$$\sigma(t,\varepsilon) = G(t) * \sigma^e(\varepsilon) \tag{4.11}$$

$$\sigma(t) = \int_{-\infty}^{t} G(t-\tau)\frac{d\sigma^e(\varepsilon)}{d\varepsilon}\frac{d\varepsilon}{d\tau}d\tau \tag{4.12}$$

The reduced relaxation function is defined as:

$$G(t) = \frac{1 + C\left[E_1\left(\frac{t}{\tau_2}\right) - E_1\left(\frac{t}{\tau_1}\right)\right]}{1 + C\ln\left(\frac{\tau_2}{\tau_1}\right)} \tag{4.13}$$

where C is the relaxation index, τ_1 is the immediate relaxation time constant, τ_2 is the long-term relaxation time constant, and $E_1(y) = \int_y^\infty \frac{e^{-z}}{z}dz$.

The elastic stress response is defined as:

$$\sigma^e(\varepsilon) = A(e^{B\varepsilon} - 1) \tag{4.14}$$

where A is the elastic stress constant and B is the elastic power constant.

Fung's QLV model has a major limitation associated with imperfect instantaneous strain that occurs during loading. Finite strain rates produce a time-dependence during the ramp time, while exceedingly short ramp times may yield lack of reproducibility. The constitutive equation is fit to the ramping and relaxation data sets until a solution converges. For a detailed QLV solution, the

reader is directed to Appendix A.

Optimization Method

The embedded MATLAB solver `lsqcurvefit` solves for the QLV coefficients $(A, B, C, \tau_1, \tau_2)$ through a least-squares fit of the final ramp and stress relaxation curve.

$$\min_x \|F(x,t) - \sigma\|_2^2 = \min_x \sum_i (F(x,t_i) - \sigma_i)^2 \tag{4.15}$$

where F is the QLV function, $x = \Big[A, B, C, \tau_1, \tau_2\Big]$, t is the time data, and σ is the stress data.

The Levenberg-Marquardt algorithm iterates from an initial solution set until global minimum is reached. Convergence is achieved once each parameter is within 10^{-10} of the optimal value.

4.4.4 Dynamic Mechanical Analysis

Under a sinusoidal strain $\varepsilon = \varepsilon_0 sin(\omega t)$ of $\omega = 2\pi f$, a viscoelastic material's stress response $\sigma = \sigma_0 sin(\omega t + \delta)$ will follow with phase lag δ, shown in Figure 4.6.

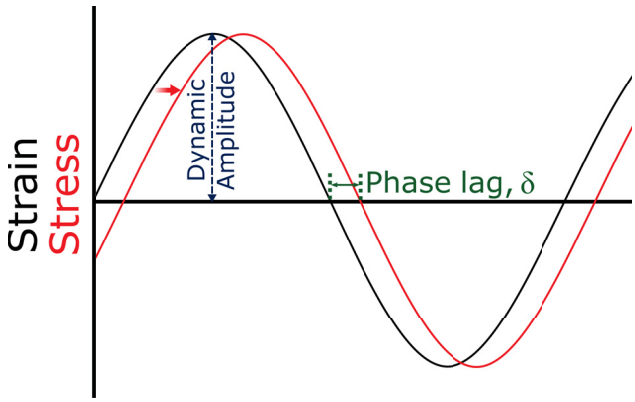

Figure 4.6: The presence of a phase lag δ is a result of viscosity in the material.

DMA quantifies the material's ability to store and dissipate tensile energy through a frequency-dependent storage (E') and loss (E'') moduli, defined in Equations (4.16) and(4.17), respectively.

$$E' = \frac{\sigma_0}{\varepsilon_0} cos\ \delta \tag{4.16}$$

$$E'' = \frac{\sigma_0}{\varepsilon_0} sin\ \delta \tag{4.17}$$

These variables provide quantitative information of the elastic and viscous components of the material, which are combined through a complex modulus, (E^*).

$$E^* = E' + iE'' \tag{4.18}$$

Vector mechanics define the ratio of loss to storage moduli as the $tan\,\delta$, a measure of energy damping.

$$tan\,\delta = \frac{E''}{E'} \tag{4.19}$$

The complex modulus magnitude and $tan\,\delta$ are calculated for [0.1-20] Hz.

4.4.5 Statistical Analysis

All averages are presented as mean ± standard deviation. One-way and two-way analyses of variance (ANOVA) and student's t-test were used to compare means of biomechanical properties across PVA compositions and among each sample type. Differences with $P < 0.05$ were considered statistically significant. Statistical analysis was performed with GraphPad Prism (V5.0, GraphPad Software Inc., San Diego, CA, USA).

Chapter 5

Results

This chapter presents the experimental results describing the stress-strain and stress relaxation behaviors of aorta, poly(vinyl alcohol), and Dacron samples. Analytic solutions of the stress relaxation curves evaluated by Fung's quasi-linear viscoelasticity theory are presented. Solved model parameters are listed. Dynamic mechanical analysis results are summarized to show frequency dependence of mechanical properties.

5.1 Cryogel Formation

PVA solution temperature in relation to the set temperature of the programmable chilling/heating plate is shown in Figure 5.1. The PVA solution successfully reaches -20°C and achieves appropriate freezing and thawing rates. Maintaining the plate in a -20°C freezer ensured an accurate freezing rate, although thawing lagged. Furthermore, a phenomena characteristic of cryostructure formation was observed during freezing. The PVA solution temperature increases approximately 4°C after the plate reaches -6°C. Subsequent cycles resulted in higher peaks occurring at lower temperatures.

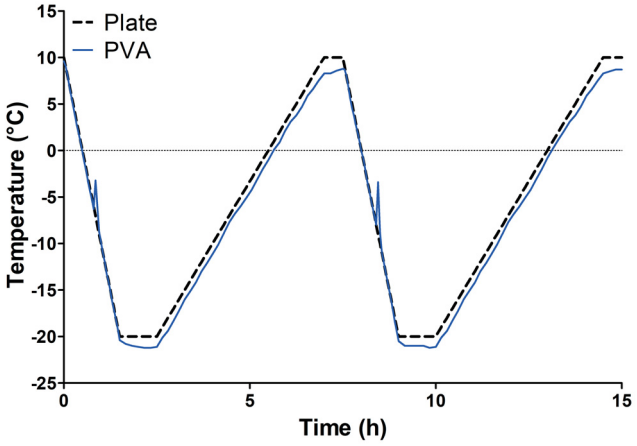

Figure 5.1: PVA temperature during freeze-thaw cycles.

5.2 Stress-Strain Behavior

Loading-unloading curves obtained by biaxial tensile experiments reveal incremental elastic moduli at various levels of strain and the viscous measure of energy loss. PVA formulations are assessed against aortic samples by these parameters.

5.2.1 Incremental Modulus

All samples tested exhibit a hyperelastic response in both directions, shown by the modulus increase at higher strains. PVA formulations closely match the incremental modulus of healthy tissue, specifically that of 20% concentration. PVA concentration has an effect on incremental modulus, although negligible at lower strains. The initial concentration of PVA solution determines the concentration of crosslinks in the resulting cryogel. This manifests in greater resistance to strain and an increasing incremental modulus. This effect is indiscriminate of direction, suggesting that crosslinks formed randomly within the cryogel.

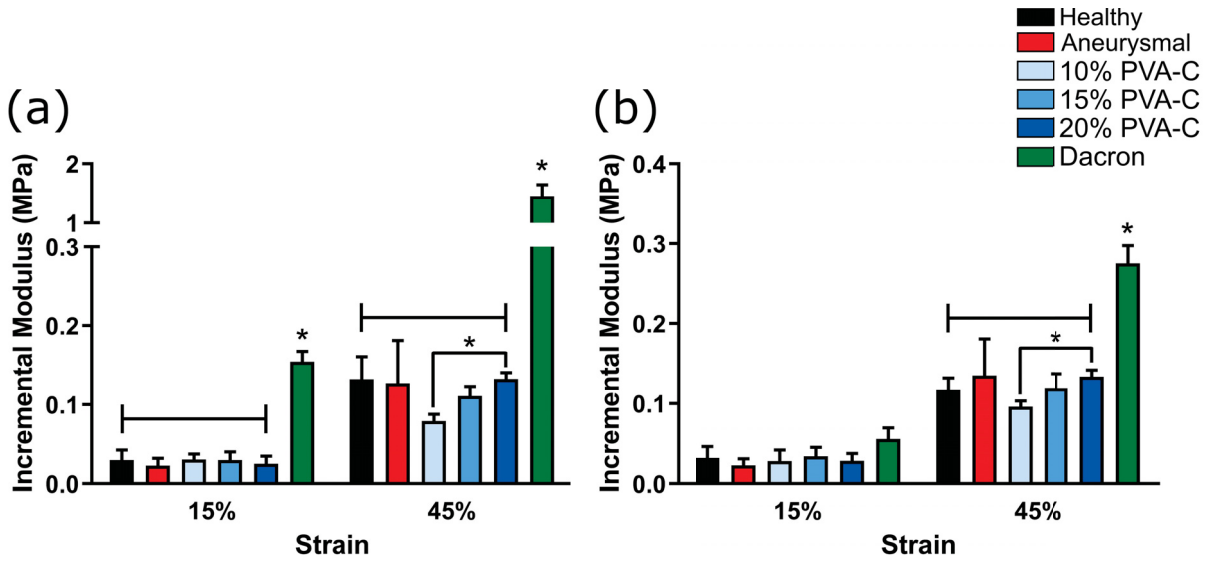

Figure 5.2: Incremental modulus at 15% and 45% strain in the **(a)** circumferential and **(b)** longitudinal directions. Chart values represent mean ± SD; $^*p < 0.05$ measured for same strain.

Dacron grafts are approximately 5- and 11-times stiffer than healthy aorta in the circumferential direction at 15% and 45% strain, respectively. In the longitudinal direction, this modulus disparity between Dacron and tissue is decreased. No significant differences were observed between samples considered healthy and aneurysmal.

5.2.2 Energy Loss

Energy loss is a viscous measure of energy absorbed by the material during testing. It provides information of the material's capacity to dissipate energy.

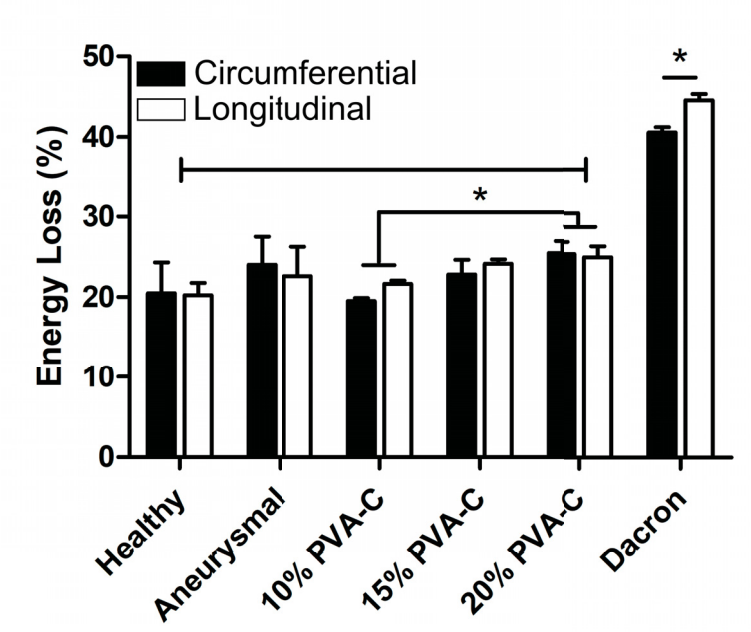

Figure 5.3: Circumferential and longitudinal energy loss of each sample. Chart values represent mean ± SD; $^*p < 0.05$ for average of both directions.

In Figure 5.3, energy loss of each sample is presented for the circumferential and longitudinal directions. Dacron grafts exhibit twice as much energy loss as healthy ascending aorta. Increases in PVA concentration also yield increased energy loss. These data suggest that initial PVA solution concentration not only affects the cryogel's stiffness at higher strains, but also contributes to its viscosity measured by energy loss. As with incremental modulus, homogeneously crosslinked cryogels exhibit comparable energy loss across both directions.

5.2.3 Effect of Freeze-Thaw Cycles

To evaluate the effect of FTCs on incremental modulus and energy loss, PVA cryogels of 6 and 12 FTCs were tested. According to Figure 5.4, cycle number and PVA concentration have comparable consequences. With increasing cycle number, both incremental modulus at 45% strain and energy loss also increase, although increases in energy loss are more drastic.

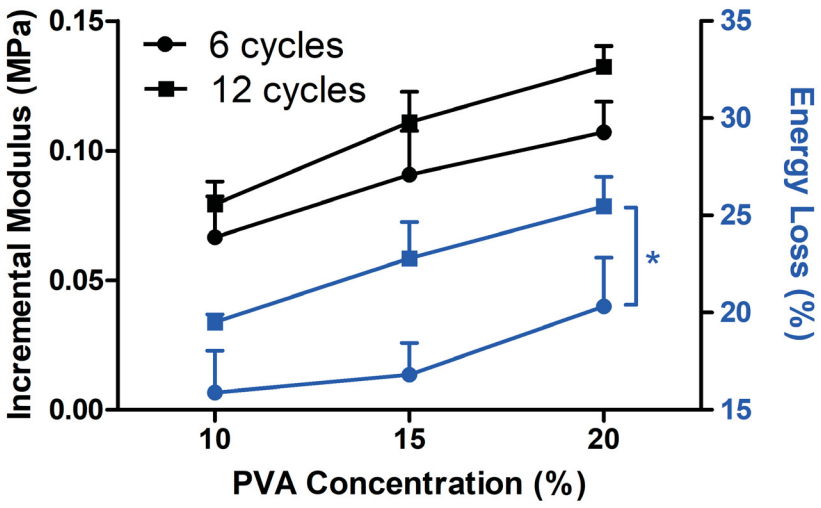

Figure 5.4: Incremental modulus (45% strain) and energy loss according to initial PVA concentration. Chart values represent mean ± SD; $^*p < 0.05$ for energy loss across all concentrations.

Since increasing PVA concentration and FTCs both independently increase crosslinks, their implementation will have similar consequences on the final PVA-C. Therefore, higher PVA concentration in the initial solution can reduce the number of FTCs required to achieve stiff mechanical properties. Similarly, both parameters can be used in tandem to refine the mechanical properties towards the desired resulting PVA-C.

5.2.4 Histology

Histologic examination of selected samples revealed noticeable differences in composition and organization among healthy and aneurysmal tissue.

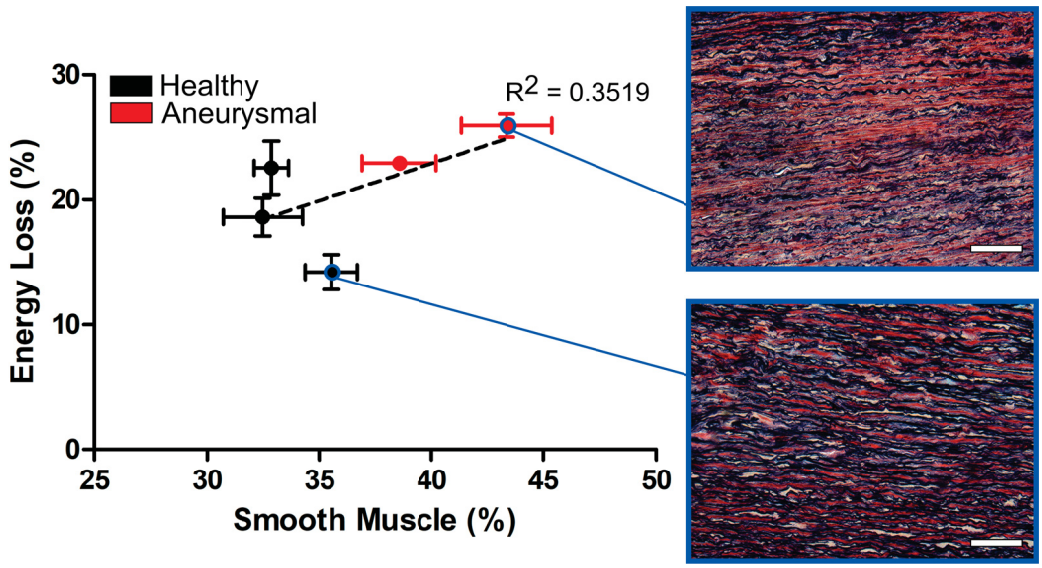

Figure 5.5: Energy loss as a function of smooth muscle present in the aortic media. Scale bar represents 100 μm.

Among the samples imaged, healthy tissue was characterized by higher elastin content, 45.3 $\pm$ 2.07% vs. 39.78 $\pm$ 1.84% in aneurysmal tissue. Thick, continuous elastinous sheets encapsulate single layers of smooth muscle inside healthy tissue. In aneurysmal tissue, several layers of smooth muscle cells are separated by weak, discontinuous elastin fibers, which vary in integrity across the thickness. Aneurysmal tissue held higher levels of smooth muscle content. A moderate correlation exists between the presence of smooth muscle and the magnitude of energy loss, which suggest that smooth muscle content alone is not an effective predictor of this viscous parameter.

Correlation of these samples with energy loss by patient age is more evident, seen in Figure 5.6. Including more samples, however, weakened this correlation. Only tissue samples with sufficient tests ($n \geq 3$) for energy loss are presented here. This data suggests that the condition or organization of smooth muscle cells may affect the tissue's viscous behavior, instead of their mere presence. Other wall constituents may also contribute to the tissue's viscoelasticity.

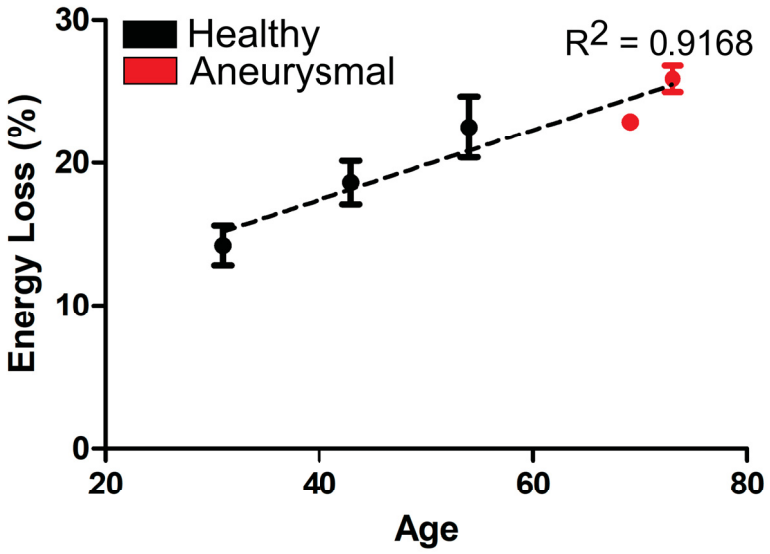

Figure 5.6: Correlation between patient age and energy loss.

5.3 Stress Relaxation

Stress relaxation preconditioning provided reproducible results of the time-dependent behavior. Similar to preconditioning performed during loading and unloading, the maximum stress attained in stress relaxation dramatically decreases after the first cycle. In Figure 5.7, normalized stress relaxation exhibits negligible differences in stress relaxation rates at five cycles.

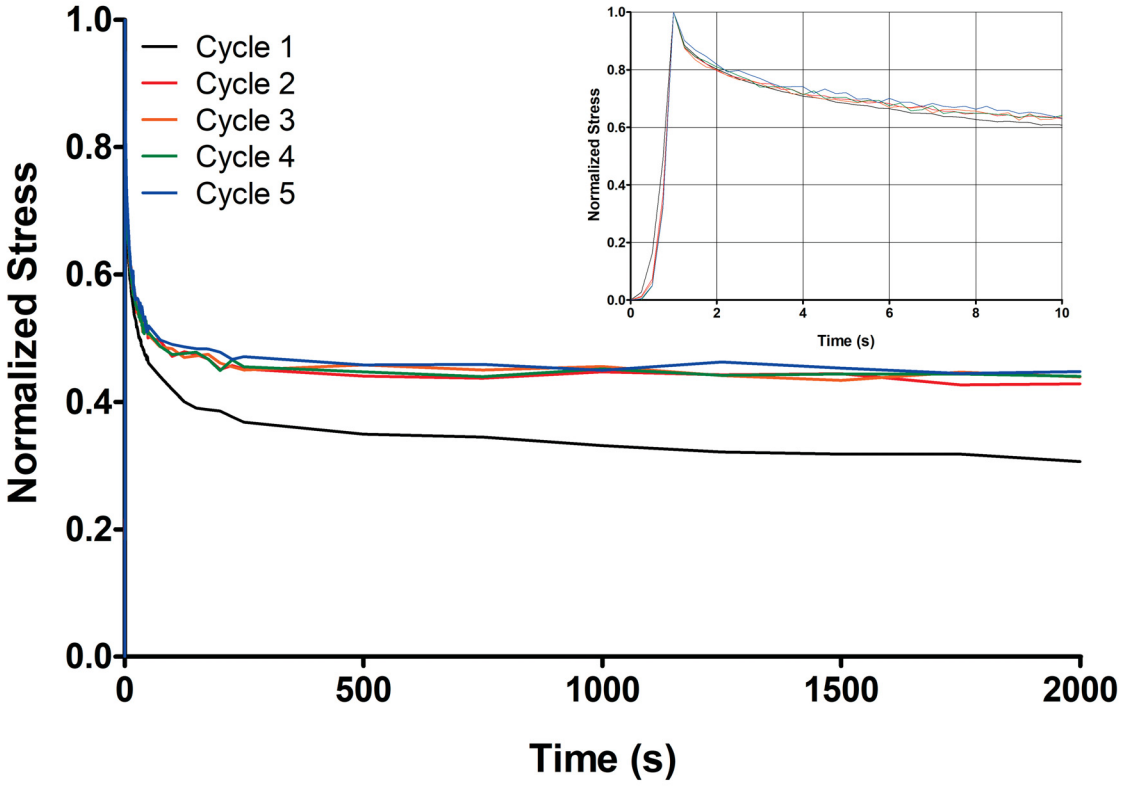

Figure 5.7: Stress relaxation preconditioning cycles yield repeatable curves in aortic tissue. Inset displays first 10 seconds.

5.3.1 QLV Model Fitting

The last stress relaxation cycle of each sample was subject to parameter estimation under the QLV platform.

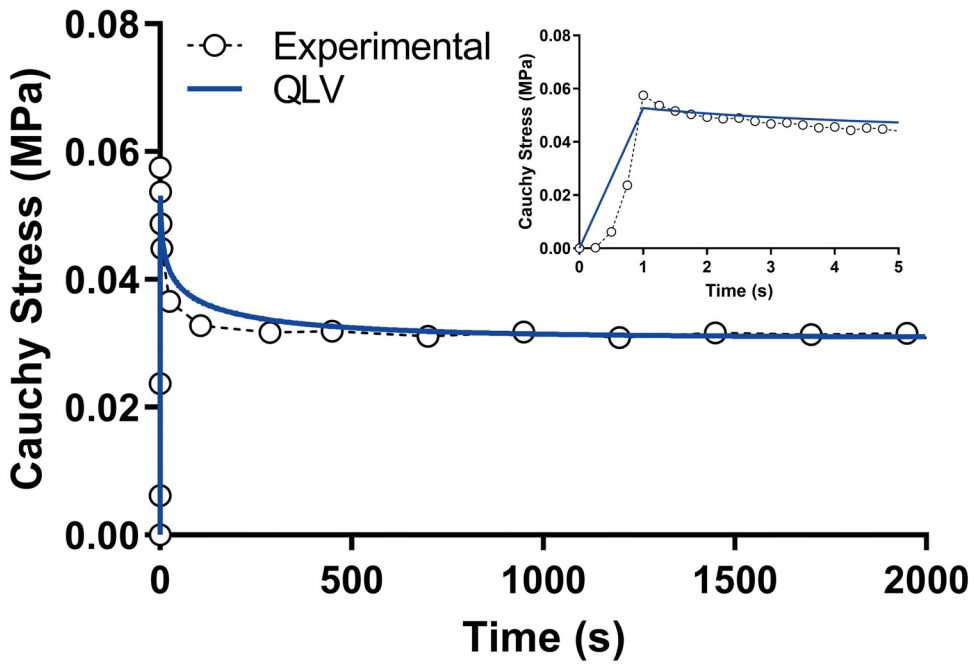

Figure 5.8: QLV model fit on typical stress relaxation of aortic tissue. Inset displays first 5 seconds.

The experimental stress relaxation exhibits a nonlinear ramp stress, marked by a stress relaxation rate that decreases over time. The QLV model is inadequate in predicting the stress levels during the ramp phase, but is able to recover in predicting the long-term relaxation. This is evidenced by the increasing residuals level during the first second, displayed in Figure 5.9. The model overestimates the material's elasticity, resulting in an underestimation of viscosity. This effect is more pronounced in materials with high elastic modulus and viscosity, such as Dacron.

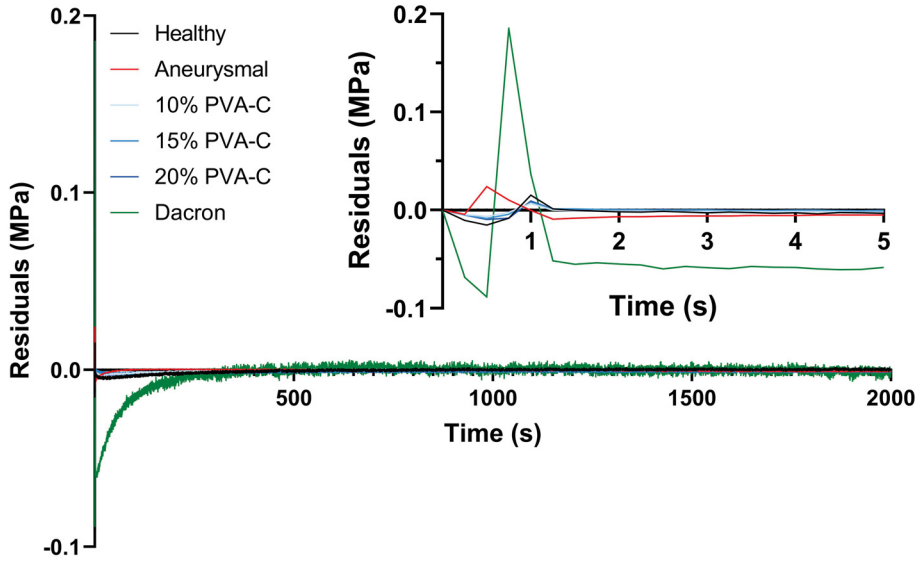

Figure 5.9: Residuals of each sample compared to their respective model fit. Inset displays first 5 seconds.

The solved QLV parameters for each sample are displayed in Table 5.1 below. Elastic parameters A and B are defined in the elastic stress function in Equation (4.14). Viscous parameters C, τ_1, and τ_2 are defined in the reduced relaxation function in Equation (4.13).

Table 5.1: QLV Parameters

	A (MPa)			**B (10^{-5})**			**C**			τ_1 (s)			τ_2 (s)		
Healthy	1984.62	±	216.41	2.94	±	0.64	0.1168	±	0.0420	0.5444	±	0.0852	825.25	±	66.331
Aneurysmal	1830.55	±	279.18	2.24	±	0.52	0.1728	±	0.0860	0.5836	±	0.1818	382.78	±	173.93
10% PVA-C	1321.69	±	105.17	2.03	±	0.28	0.1524	±	0.0537	0.5277	±	0.0734	628.30	±	79.643
15% PVA-C	1616.69	±	182.10	1.64	±	0.22	0.1172	±	0.0815	0.5075	±	0.0821	648.46	±	108.40
20% PVA-C	1716.57	±	212.07	2.16	±	0.45	0.1630	±	0.0667	0.4491	±	0.0382	890.65	±	4.7221
Dacron	5222.69	±	200.83*	9.30	±	1.18*	0.4845	±	0.1166*	0.3445	±	0.0727	195.05	±	32.614*

Parameter values for circumferential direction presented as mean ± SD; $^*p < 0.05$ for each parameter across all groups.

The QLV model has overestimated the material's elastic modulus and did not effectively account for the hyperelastic behavior under 60% strain in a 1 second rise time. Therefore, parameter A estimates a much stiffer material and parameter B is negligible across all groups. However, average differences in overall stiffness are still noticeable across parameter A. The parameter C represents a measure of viscosity within the material and τ_1 and τ_2 represent the immediate and long-term time constants, respectively. Dacron holds the highest initial relaxation rate and the lowest normalized level of remaining stress, resulting in the largest estimation of C. Dacron also reaches its final value much quicker, confirmed by a shorter time constant τ_2.

PVA formulations and aortic tissue respond similarly under stress relaxation according to the

QLV model. Increasing PVA concentration resulted in a shorter τ_1 and a longer τ_2, although not statistically different. No observable trend was seen in material constant C, confirming the consistent relaxation behavior of PVA cryogels. No differences in this constant between tissue and PVA-C implies that the initial relaxation rate and final relaxation level is similar.

5.4 Dynamic Mechanical Analysis

Dynamic mechanical analysis (DMA) is required to understand how the material behaves under a variety of frequencies. In the aortic wall, these frequencies range from pulsatile loads to high frequency vibrations. The complex modulus is a measure of stiffness accounting for contributions from the elastic and viscous components of the material. The complex modulus magnitude, seen in Figure 5.10, is relatively independent of frequency. As expected, increasing PVA concentration also increases complex modulus. In this case, 15% PVA-C is within range of aortic tissue at physiological frequencies.

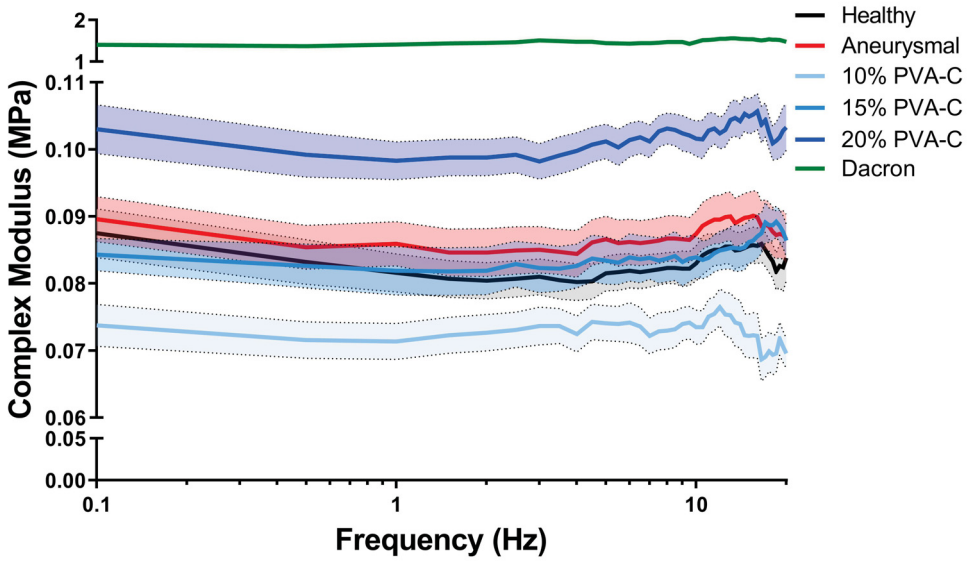

Figure 5.10: Complex modulus is frequency-independent from [0.1-20] Hz in all samples.

To differentiate the elastic and viscous contributions of the complex modulus, $tan\,\delta$ is presented in Figure 5.11. This parameter represents a ratio of loss to storage modulus, or viscous to elastic components. All samples exhibit a similar trend. The viscous component of most samples reaches a minimum between [1-3] Hz. All PVA cryogels exhibit similar frequency-dependent viscous behavior of aortic tissue.

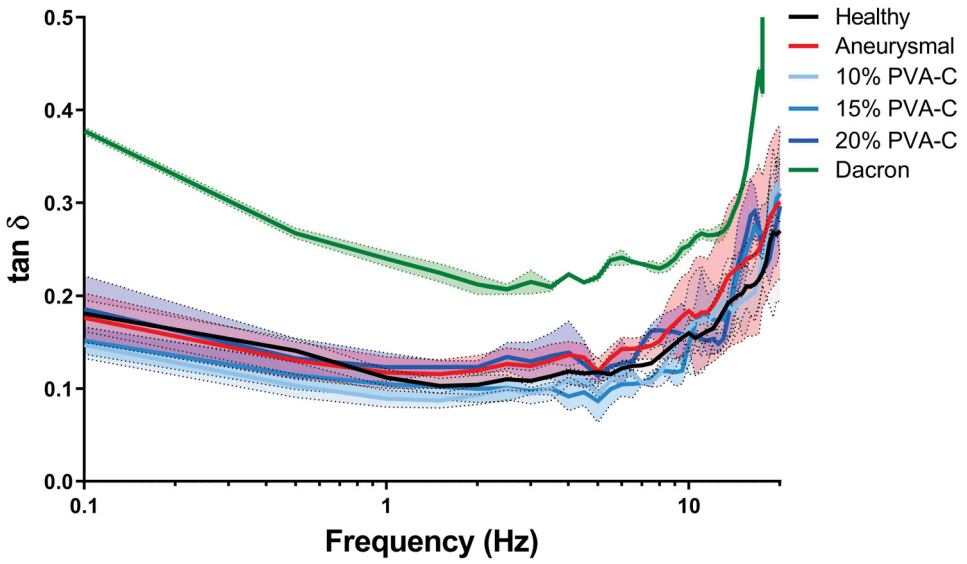

Figure 5.11: Contribution of viscosity to the complex modulus follows similar frequency-dependent trends in all samples.

Measurements after 10 Hz increase in variability, most likely due to the contribution of vibrations within the saline solution containing the sample. This could explain the unexpected sudden decrease in complex modulus at high frequencies.

Chapter 6

Discussion

This work proposed the use of PVA-C as a mechanically viable substitute for ascending aorta. Viscoelastic properties of various PVA-C compositions were compared to those of human ascending aorta. The ease of manufacturability in acquiring reproducible properties compels further investigation into PVA-C as a vascular prosthesis over Dacron grafts.

Cryogel Formation

During formation of the cryogel, gel temperature revealed a characteristic trend. Upon freezing, a heat emission peak occurred between -6 and -10°C, which correlates to regions of increased crystalline domains and hydrogen bond formation [62, 128]. As crystallization increased with more cycles, the heat emission peak also increased. Solutions of varying PVA concentrations underwent identical freeze-thaw regimens and were subject to tensile experiments to isolate the effect of PVA concentration on final cryogel stiffness.

Elastic Response

Aortic tissue increases in stiffness as it is stretched. This hyperelasticity is also revealed in Dacron, although its magnitude of stiffness is much higher. PVA-C is able to replicate the nonlinear stress-strain behavior at low and high strains. Incremental modulus at 45% strain correlates to physiological moduli at the transition between elastin and collagen load-bearing in the rat aorta [53]. Aortic tissue and Dacron incremental modulus values are consistent with the literature [65, 191]. PVA-C maintains the stiffness of aortic tissue at physiological strain. In other words, the compliance of this artificial tissue matches that of the aortic wall. Furthermore, increasing PVA concentration yields stiffer cryogels [127, 204]. This effect is rather negligible under low strain.

The cryogels prepared in this work are isotropic, due to its uninhibited crystallization during FTCs. The distinct wall layers of the aorta classify the material as cylindrically orthotropic. In a biaxial tensile test, healthy ascending aortic tissue samples display a level of anisotropy [46, 191]. Millon et al. successfully achieved anisotropic PVA-C by applying an initial strain after a single FTC [139]. Subsequent FTCs were performed under a strained cryogel to induce a non-homogenous

crystal structure. This technique can be considered to recreate the direction-dependent behavior of the aortic wall.

Energy Loss

Energy loss is a measure that describes how aortic tissue distributes energy. During each cardiac cycle, the aortic wall receives energy from the pumping heart with each ventricular ejection of blood. The aortic wall absorbs this energy by distending. In accordance with its Windkessel function, the wall returns to its resting circumference, transferring energy back to the blood. In this process, the aortic wall dissipates some energy into itself. While systolic pressure rises rapidly, diastolic pressure returns in a much slower fashion. This is due to the reduced energy returned by the wall in diastole [212]. Although the tissue's compliance enables the Windkessel function, the tissue's dissipative capacity directs its timing. Energy loss is a reproducible, quantitative measure of the tissue's dissipative capacity through hysteresis observed in standard biaxial testing. Energy loss has been a useful biomechanical parameter that correlates with microstructural defects in the media [46, 47].

The behavior of this hysteresis loop has been thoroughly observed *in vitro* and *in vivo*. Unlike the loading curve, the unloading curve is moderately unaffected by changes in the strain or strain rate [76]. Therefore, the width of the hysteresis loop is determined by the magnitude of stretch or strain rate [166]. When considering the function of the aortic wall, this response is expected. As the tissue experiences higher levels of stress, it demands increasingly more relaxation to restore the tissue to its residual stress state. Pressure-area dynamics of the aorta can be obtained *in vivo* by mapping the stress and strain of the tissue under physiological loading cycles [98, 184]. Armentano et al. quantified the viscous component of the aortic wall by analyzing *in vivo* hysteresis loops in conscious dogs [12]. The study confirmed that the viscous modulus depends not only on smooth muscle activation, but also on the arterial pressure magnitude.

Under physiologic loads, the PVA cryogels maintain similar energy dissipating properties as aortic tissue. Initial PVA concentration affects the extent of energy loss, although it is unclear whether this is due to increased chain interactions in the gel or the higher stress level achieved by more crosslinks. Similarly, the dependence of viscosity on stress level may account for the increased energy loss in Dacron, which achieved supraphysiologic loads at 60% strain.

Stress Relaxation

While energy loss is a robust parameter and hysteresis loops are observed *in vivo*, it provides little information of the time-dependent behavior under a peak load. In standard biaxial tests, unloading is performed at a controlled rate. In physiological loading conditions, the aortic wall's unloading is determined by its previous distension, heart rate, and smooth muscle activation. For this reason, stress relaxation tests were performed to assess viscoelastic behavior over a time span, where unloading is achieved by the material alone.

Multiple stress relaxation cycles preconditioned the material to achieve repeatable curves. Carew et al. determined that repeatable stress relaxation curves in porcine aortic valves cannot be achieved by standard loading-unloading preconditioning [39]. Zou et al. adopted this method on aortic elastin, compensating each cycle for drops in initial stress level by modifying the target stretch [219]. In this study, the material's initial stress level dropped significantly after the first cycle, just as it does in standard preconditioning protocols. However, the maximum stretch was kept consistent through all cycles. Excised aorta achieved up to 50% relaxation in this study after 5 cycles, which is substantially larger than the 20% relaxation observed by Zou et al. This marked increase may be due to the strain-rate dependence of viscoelasticity in soft tissues [61]. In this study, samples achieved target stretch in half the time as those in the study by Zou et al.

Quasi-linear viscoelasticity theory is a popular method to model viscoelastic behavior of biological tissues [38, 61, 113]. Adaptations to this model have been used to characterize aortic elastin stress relaxation and creep [219]. Viscoelastic modeling under the QLV platform has been applied to *in vivo* and *ex vivo* pressure-area hysteresis loops in the aorta [198]. While the QLV model is widely used, it improperly assumes that strain and time effects on stress are independent. For this reason, it insufficiently simulates the magnitude of initial stress relaxation in these tests. The immediate relaxation time constant, τ_1, is not as robust a measure as the long-term time constant, τ_2. Stress relaxation tests experienced 60% strain in 1 second to achieve a near-instantaneous step strain. High strain rates lead to amplified stress levels, while low strain rates risk relaxation occurring during stretching. The accuracy of the ramp stress was also limited. Despite attempting various discretizations, the QLV model could only attain accurate ramp results if the relaxation portion of the piecewise function was omitted. To account for the rapid initial stress relaxation, the QLV underestimates the peak stress and does not simulate hyperelasticity. Increasing the amount of iterations had little effect. Zou et al. had similar difficulty with a ramp time of 2 seconds. Adaptive and discrete QLV models have been developed to link the stress relaxation behavior to strain or time-independence [15, 148].

PVA cryogels and ascending aorta have comparable initial stress levels under 60% strain, and residuals from QLV modeling are similar. Stiffer PVA cryogels exhibit a shorter τ_1 and longer τ_2. Aortic tissue is less predictable. QLV is the least accurate model for Dacron because initial stress relaxation is highest in this material. Although viscoelasticity in Dacron is significantly higher than aortic tissue, such high stress levels are not expected *in vivo*.

Frequency Response

Dynamic mechanical analysis provides detail of the material's frequency dependent properties. Aortic tissue is subject to a variety of strain rates within its pressure waveform and these can be modified by heart rate. Although standard biaxial testing provides robust biomechanical quantities for material comparison, it does not effectively determine properties at physiologically relevant frequencies. Testing samples were subjected to cycles at [0.1-20] Hz ranging from 10-60% strain. Over this range, complex modulus was frequency-independent in all samples, with healthy aorta

measured at approximately 80 kPa. This frequency-independent trend is consistent with Bergel's evaluation [26]. Bergel also observed a slight increase in viscosity after 5 Hz. In the octopus aorta, Shadwick and Gosline noticed a quicker increase in viscosity after 1 Hz [177]. Apter and Marquez found a steep increase in $tan\,\delta$, approaching an asymptote at 10 Hz [11]. These studies vary in strain level and pressure level affects aortic dynamic viscoelasticity [119].

The results of this study reveal a noticeable increase in $tan\delta$ after 5 Hz with a valley between [1-3] Hz, most closely resembling the results seen by Shadwick and Gosline. Examination of coronary arteries with a similar DMA setup as the one used in this study was not able to observe resonance up to 12 Hz [36]. Nonetheless, Apter and Marquez observed an aortic resonance frequency at 5 Hz, at which phase shift δ reached 90°. Although the viscous increase was not observed to the same extent, all aortic samples in this study resembled this increasing trend. When considering the function of the aortic Windkessel, the results are enlightening. Viscosity hinders Windkessel function by limiting energy storage capacity attributed to its elasticity. At physiological frequencies of forward pressure waves at [1-3] Hz, viscous properties approach a minimum. At low and high frequencies possibly caused by faster reflected waves or vibrations, wall viscosity increases to dissipate energy. Simulations of pulse wave attenuations in the arterial tree reveal damping occurs as a result of viscosity in the material [135, 137, 173]. The amount of dissipation decreases with increased longitudinal stress or transmural pressure. Most simulations that include reflected waves simplify the amount of bifurcations present. Local blood flow disturbances, such as those induced by Dacron implantation, can contribute to pulse wave irregularity.

The DMA experiments conducted were uniaxial. Controlling longitudinal stress during DMA tests is expected to have a more pronounced effect for Dacron, which is the stiffest material. However, PVA cryogels and aortic tissue exhibit similar longitudinal stress behaviors. PVA-C effectively mimics aortic viscous behavior across the frequency sweep. Theoretically, these materials will be able to fulfill the aortic tissue's balance of Windkessel and pulse attenuation.

Histology

Histological examination revealed noticeable disparities between healthy and aneurysmal tissue. Smooth muscle concentration was not an independent predictor of tissue's viscosity measured by energy loss. Among the small size of five samples observed, increased collagen-to-elastin ratio and energy loss were also correlated ($R^2 = 0.8369$). Collagen-to-elastin ratio signifies the tissue's effective age. Smooth muscle cells in tissues with a lower C/E ratio may hold higher integrity than those with a higher C/E ratio. High stresses caused by increased collagen concentration may cause degradation of smooth muscle cells' relaxation properties over time. Conversely, elastin degradation may increase load-bearing responsibility of smooth muscle cells, also inducing cell fatigue. Further investigation of smooth muscle mechanotransduction and pathophysiology is required to support this assertion. Nonetheless, smooth muscle content is not the sole determinant of arterial viscoelastic properties.

6.1 Limitations

Viscoelasticity is a complex behavior that is not only time-dependent, but also strain- and stress-dependent. Isolating these effects are challenging when assessing a variety of materials. In this study, strain rate was controlled in all experiments. This results in a variety of stress levels that rely on the material and the sample's dimensions. Stress-level dependence on viscoelasticity must be considered when evaluating aortic tissue and polymers. Excluding Dacron, a 60% strain achieved physiological Cauchy stress levels, for which viscoelastic properties can be moderately compared. Dacron's large increase in stress levels at the same strain may explain its proportionately higher viscosity observed in this study. Hasegawa and Azuma verified that Dacron grafts stretched to 10% matched viscoelasticity of the proximal aorta stretched to 50% strain [84]. Amabili et al. found that Dacron loss factor decreased with pre-stretch and achieved a magnitude and frequency response similar to those of aortic tissue in this study [8]. The study by Amabili et al., however, used a dynamic amplitude of 0.3% strain compared to the 25% strain used in this study. Despite this limitation of Dacron, this study effectively focused on the comparison between aorta and PVA-C formulations. Dacron's energy loss and $tan\,\delta$ values do not resemble *in vivo* behavior, but further attests to its drastically lower compliance. A confounding factor in the aortic tissue is the variation in smooth muscle viability among samples. Increasing the amount of samples would help to eliminate these variable effects. Understanding the *in vivo* pressure dynamics and pressure wave velocity would help provide detail into the potential fatigue of smooth muscle function in the thoracic aorta. Measuring the distance from the aortic valve and accounting for regional location of the tested sample may help illuminate reasons for potential variation across tissues.

6.2 Future Work

Biaxial tensile tests are simple and reproducible, which help in providing a standard for material characterization. They do not mimic the conditions that the aorta endures *in vivo*. Stress relaxation and dynamic mechanical analysis incorporate time-dependent behaviors, but are still insufficient. A more sophisticated closed-loop system that accounts for transmural pressure, characteristic impedance, and physiological frequency can be replicated with a pulsatile blood pump flowing through a conduit. To confirm the results here, aortic rings, cylindrical PVA-C, and Dacron grafts should be assessed in this scenario.

New processing techniques can be attempted to modify the architecture of PVA cryogels. A structure of individual layers can be cast or 3-D printed. An outside layer can mimic the adventitial resistance to deformation and provide suture sites for implantation. PVA is a versatile material that can be manipulated to appropriate aortic geometry and thickness. Aortic graft designs should be applied to this suitable material.

Chapter 7

Conclusion

This thesis examines the viscoelastic properties of poly(vinyl alcohol) cryogels and compares it to those of aortic tissue. In the same way that PVA-C hyperelasticity can be modified by polymer concentration and freeze-thaw cycle processing, viscous behavior can also be adjusted. Smooth muscle in the ascending aorta dissipates arterial pulse waves and preserves the aortic wall, but also directs the precise timing of Windkessel function. Viscosity of aortic tissue and PVA-C are achieved by distinct means, yet maintain comparable behavior at similar stress levels and frequencies. PVA-C energy loss, stress relaxation, and $tan\,\delta$ match aortic tissue, while holding identical compliance. The ease of manufacturability and versatility of mechanical properties advocate for the future of personalized grafts that match aortic geometry and maintain viscoelastic continuity along the aortic column. Current Dacron graft implantation, despite its high patency rates in the ascending aorta, yields detectable and harmful consequences to the arterial circulation as a result of its disparate geometry and mechanical properties. In the ascending aorta, PVA cryogels should be considered for the development of novel grafts to limit hemodynamic disturbances, maintain characteristic impedance, and promote Windkessel function.

Appendix A

Quasi-linear Viscoelasticity Theory

The quasi-linear viscoelastic constitutive equation begins with a stress response function that depends on both the time and strain.

$$\sigma(t,\varepsilon) = G(t) * \sigma^e(\varepsilon) \tag{A.1}$$

The Boltzmann superposition principle permits this equation to be written in the form of a linear convolution integral, terming this theory *quasi-linear*. This integral accounts for the strain history of the stress response.

$$\sigma(t) = \int_{-\infty}^{t} G(t-\tau)\frac{d\sigma^e(\varepsilon)}{d\varepsilon}\frac{d\varepsilon(\tau)}{d\tau}d\tau \tag{A.2}$$

Fung proposed a reduced relaxation function, $G(t) = \dfrac{\sigma(t)}{\sigma(0)}$, where $\sigma(t)$ represents the stress response to a step change in strain, ε [42].

$$G(t) = \frac{1 + C\left[E_1\left(\dfrac{t}{\tau_2}\right) - E_1\left(\dfrac{t}{\tau_1}\right)\right]}{1 + C\ln\left(\dfrac{\tau_2}{\tau_1}\right)} \tag{A.3}$$

where $E_1(y) = \int_y^\infty \dfrac{e^{-z}}{z}dz$ and C, τ_1, and τ_2 are viscoelastic material constants, such that $\tau_1 \ll \tau_2$.

The material constant C describes the initial relaxation rate and the final relaxation value, while τ_1 and τ_2 refer to the immediate ($t = {t_0}^+$) (see Figure A.1) and long-term ($t = \infty$) constants, respectively.

The instantaneous elastic response, $\sigma^e(\varepsilon)$, represents the stress response to a step change in strain, ε. Unlike the relaxation function, the elastic response does not account for strain history since loading is assumed to occur at a high strain rate (step change). The following exponential approximation was proposed by Woo [213] and has been considered for aortic valve leaflets [38].

$$\sigma^e(\varepsilon) = A(e^{B\varepsilon} - 1) \tag{A.4}$$

where A and B are elastic material constants.

The QLV model must be fit for stress relaxation data, shown as Figure A.1, to determine the material parameters.

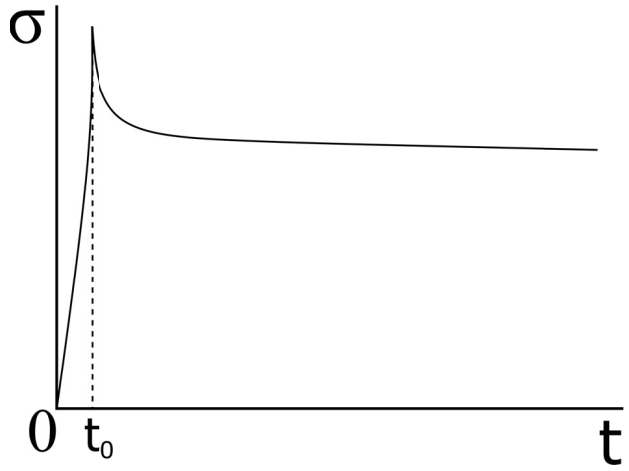

Figure A.1: High loading rate begins at $t = 0$ and ends at $t = t_0$.

The stress response integral requires $G(t-\tau)$ and $\dfrac{d\sigma^e(\varepsilon)}{d\varepsilon}$. First, solve for $G(t-\tau)$:

$$G(t-\tau) = \frac{1 + C\left[E_1\left(\dfrac{t-\tau}{\tau_2}\right) - E_1\left(\dfrac{t-\tau}{\tau_1}\right)\right]}{1 + C\ln\left(\dfrac{\tau_2}{\tau_1}\right)} \tag{A.5}$$

where $E_1\left(\dfrac{t-\tau}{\tau_i}\right) = \displaystyle\int_{\frac{t-\tau}{\tau_i}}^{\infty} \frac{e^{-z}}{z} dz$ for $i = [1, 2]$.

In MATLAB, the exponential function E_1 is replicated by `expint`.

Next, solve for $\dfrac{d\sigma^e(\varepsilon)}{d\varepsilon}$:

$$\frac{d\sigma^e(\varepsilon)}{d\varepsilon} = \frac{d}{d\varepsilon} A(e^{B\varepsilon} - 1) \tag{A.6}$$

$$= ABe^{B\varepsilon} \tag{A.7}$$

$$= ABe^{B\dot{\varepsilon}\tau} \tag{A.8}$$

Finally, plug Equations (A.5) and (A.8) into Equation (A.2).

$$\sigma(t) = \int_{-\infty}^{t} \frac{1 + C\left[E_1\left(\frac{t-\tau}{\tau_2}\right) - E_1\left(\frac{t-\tau}{\tau_1}\right)\right]}{1 + C\ln\left(\frac{\tau_2}{\tau_1}\right)} AB e^{B\dot{\varepsilon}\tau} \frac{d\varepsilon(\tau)}{d\tau} d\tau \tag{A.9}$$

$$= \frac{AB\dot{\varepsilon}}{1 + C\ln\left(\frac{\tau_2}{\tau_1}\right)} \int_{-\infty}^{t} d\tau e^{B\dot{\varepsilon}\tau} \left[1 + C\left[E_1\left(\frac{t-\tau}{\tau_2}\right) - E_1\left(\frac{t-\tau}{\tau_1}\right)\right]\right] \tag{A.10}$$

Integration limits are adjusted to correct for strain history starting at $t = 0$. The stress response during ramp ($0 < t < t_0$) and stress relaxation ($t \geq t_0$) holds different integration limits to distinguish when loading ceases. A piecewise function is loaded into MATLAB.

$$\sigma(t) = \frac{AB\dot{\varepsilon}}{1 + C\ln\left(\frac{\tau_2}{\tau_1}\right)} \int_{0}^{t} d\tau e^{B\dot{\varepsilon}\tau} \left[1 + C\left[E_1\left(\frac{t-\tau}{\tau_2}\right) - E_1\left(\frac{t-\tau}{\tau_1}\right)\right]\right], \qquad \{0 < t < t_0\} \tag{A.11}$$

$$\sigma(t) = \frac{AB\dot{\varepsilon}}{1 + C\ln\left(\frac{\tau_2}{\tau_1}\right)} \int_{0}^{t_0} d\tau e^{B\dot{\varepsilon}\tau} \left[1 + C\left[E_1\left(\frac{t-\tau}{\tau_2}\right) - E_1\left(\frac{t-\tau}{\tau_1}\right)\right]\right], \qquad \{t \geq t_0\} \tag{A.12}$$

where $E_1\left(\frac{t-\tau}{\tau_i}\right) = \int_{\frac{t-\tau}{\tau_i}}^{\infty} \frac{e^{-z}}{z} dz$ for $i = [1, 2]$.

Bibliography

[1] Aorte. *Smart Servier Medical Art*.

[2] *Anatomy & Physiology*. OpenStax CNX, Feb 26, 2016, ch. 20.

[3] Abbott, W. M., Megerman, J., Hasson, J. E., L'Italien, G., and Warnock, D. F. Effect of compliance mismatch on vascular graft patency. *Journal of Vascular Surgery 5*, 2 (1987), 376–382.

[4] Adams, J. D., Garcia, L. M., and Kern, J. A. Endovascular repair of the thoracic aorta. *Surgical Clinics 89*, 4 (2009), 895–912.

[5] Alexandre, N., Ribeiro, J., Gärtner, A., Pereira, T., Amorim, I., Fragoso, J., Lopes, A., Fernandes, J., Costa, E., Santos-Silva, A., et al. Biocompatibility and hemocompatibility of polyvinyl alcohol hydrogel used for vascular grafting - in vitro and in vivo studies. *Journal of Biomedical Materials Research Part A 102*, 12 (2014), 4262–4275.

[6] Alfonso, M., Cymberknop, L. J., Suárez, D., Castillo, F. G., and Armentano, R. L. Elastic mismatch between ePTFE and PLLA vascular grafts in relation to femoral and carotid arteries in humans: in vivo, in vitro and in silico assessment. *Health and Technology 6*, 3 (2016), 181–187.

[7] Allaire, E., and Clowes, A. Endothelial cell injury in cardiovascular surgery: the intimal hyperplastic response. *The Annals of Thoracic Surgery 63*, 2 (1997), 582.

[8] Amabili, M., Balasubramanian, P., Breslavsky, I., Ferrari, G., and Tubaldi, E. Viscoelastic characterization of woven Dacron for aortic grafts by using direction-dependent quasi-linear viscoelasticity. *Journal of the Mechanical Behavior of Biomedical Materials 82* (2018), 282–290.

[9] Appleyard, R. F., and Sauvage, L. R. Haemodynamic consequences of arterial replacement with a synthetic graft. *Cardiovascular Research 20*, 1 (1986), 26–35.

[10] Apter, J., Rabinowitz, M., and Cummings, D. Correlation of visco-elastic properties of large arteries with microscopic structure. *Circulation Research 19* (1966), 104–121.

[11] Apter, J. T., and Marquez, E. Correlation of Visco-Elastic Properties of Large Arteries with Microscopic Structure. *Circulation Research 22*, 3 (1968), 393–404.

[12] Armentano, R. L., Barra, J. G., Levenson, J., Simon, A., and Pichel, R. H. Arterial wall mechanics in conscious dogs: Assessment of viscous, inertial, and elastic moduli to characterize aortic wall behavior. *Circulation Research 76*, 3 (1995), 468–478.

[13] Azadani, A. N., Chitsaz, S., Mannion, A., Mookhoek, A., Wisneski, A., Guccione, J. M., Hope, M. D., Ge, L., and Tseng, E. E. Biomechanical Properties of Human Ascending Thoracic Aortic Aneurysms. *The Annals of Thoracic Surgery 96*, 1 (2013), 50 – 58.

[14] Azuma, T., and Hasegawa, M. A Rheological Approach to the Architecture of Arterial Walls. *The Japanese Journal of Physiology 21*, 1 (1971), 27–47.

[15] Babaei, B., Abramowitch, S. D., Elson, E. L., Thomopoulos, S., and Genin, G. M. A discrete spectral analysis for determining quasi-linear viscoelastic properties of biological materials. *Journal of The Royal Society Interface 12*, 113 (2015).

[16] Babu, A. R., Byju, A. G., and Gundiah, N. Biomechanical properties of human ascending thoracic aortic dissections. *Journal of Biomechanical Engineering 137*, 8 (2015), 081013.

[17] Bagnasco, D. S., Ballarin, F. M., Cymberknop, L., Balay, G., Negreira, C., Abraham, G., and Armentano, R. Elasticity assessment of electrospun nanofibrous vascular grafts: A comparison with femoral ovine arteries. *Materials Science and Engineering: C 45* (2014), 446 – 454.

[18] Baikoussis, N. G., Antonopoulos, C. N., Papakonstantinou, N. A., Argiriou, M., and Geroulakos, G. Endovascular stent grafting for ascending aorta diseases. *Journal of Vascular Surgery 66*, 5 (2017), 1587 – 1601.

[19] Ballyk, P. D., Walsh, C., Butany, J., and Ojha, M. Compliance mismatch may promote graftartery intimal hyperplasia by altering suture-line stresses. *Journal of Biomechanics 31*, 3 (1997), 229 – 237.

[20] Bank, A. J., Kaiser, D. R., Rajala, S., and Cheng, A. Y. In vivo human brachial artery elastic mechanics: Effects of smooth muscle relaxation. *Circulation 100*, 1 (1999), 41–7.

[21] Barra, J. G., Armentano, R. L., Levenson, J., Fischer, E., Pichel, R. H., and Simon, A. Assessment of smooth muscle contribution to descending thoracic aortic elastic mechanics in conscious dogs. *Circulation Research 73*, 6 (1993), 1040–1050.

[22] Bassiouny, H. S., Lieber, B. B., Giddens, D. P., Xu, C., Glagov, S., and Zarins, C. K. Quantitative inverse correlation of wall shear stress with experimental intimal thickening. In *American College of Surgeons Surgical Forum* (1988), vol. 39, pp. 328–330.

[23] Bassiouny, H. S., White, S., Glagov, S., Choi, E., Giddens, D. P., and Zarins, C. K. Anastomotic intimal hyperplasia: mechanical injury or flow induced. *Journal of Vascular Surgery 15*, 4 (1992), 708–717.

[24] Belz, G. G. Elastic properties and Windkessel function of the human aorta. *Cardiovascular Drugs and Therapy 9*, 1 (1995), 73–83.

[25] Bentall, H., and De Bono, A. A technique for complete replacement of the ascending aorta. *Thorax 23*, 4 (1968), 338–339.

[26] Bergel, D. H. The dynamic elastic properties of the arterial wall. *The Journal of Physiology 156*, 3 (1961), 458–469.

[27] Bergel, D. H. The static elastic properties of the arterial wall. *The Journal of Physiology 156*, 3 (1961), 445–457.

[28] Berger, K., and Sauvage, L. Late fiber deterioration in Dacron arterial grafts. *Annals of Surgery 193*, 4 (1981), 477.

[29] Berridge, D., Al-Kutoubi, A., Mansfield, A., Nicolaides, A., and Wolfe, J. Thrombolysis in arterial graft thrombosis. *European Journal of Vascular and Endovascular Surgery 9*, 2 (1995), 129 – 132.

[30] Bia, D., Aguirre, I., Zócalo, Y., Devera, L., Fischer, E. C., and Armentano, R. Regional differences in viscosity, elasticity, and wall buffering function in systemic arteries: Pulse wave analysis of the arterial pressure-diameter relationship. *Revista Española de Cardiología 58*, 2 (2005), 167–174.

[31] Bia, D., Armentano, R. L., Grignola, J. C., Craiem, D., Zócalo, Y. A., Ginés, F. F., and Levenson, J. The vascular smooth muscle of great arteries: Local control site of arterial buffering function? *Revista Española de Cardiología 56*, 12 (2003), 1202–1209.

[32] Bia, D., Zócalo, Y., Cabrera-Fischer, E. I., Wray, S., and Armentano, R. L. Quantitative analysis of the relationship between blood vessel wall constituents and viscoelastic properties: Dynamic biomechanical and structural in vitro studies in aorta and carotid arteries. *Physiology Journal 2014* (2014).

[33] Boland, E. D., Matthews, J. A., Pawlowski, K. J., Simpson, D. G., Wnek, G. E., and Bowlin, G. L. Electrospinning collagen and elastin: preliminary vascular tissue engineering. *Frontiers in Bioscience 9* (2004), 1422 – 1432.

[34] Bonow, R., Mann, D., Zipes, D., and Libby, P. *Braunwald's Heart Disease: A Textbook of Cardiovascular Medicine*. Elsevier Science, 2011.

[35] Burton, A. C. Relation of structure to function of the tissues of the wall of blood vessels. *Physiological Reviews 34*, 4 (1954), 619–642.

[36] Burton, H. E., Freij, J. M., and Espino, D. M. Dynamic viscoelasticity and surface properties of porcine left anterior descending coronary arteries. *Cardiovascular Engineering and Technology 8*, 1 (2017), 41–56.

[37] Bustos, C. A., Herrera, C. M. G., and Celentano, D. J. Modelling and simulation of the mechanical response of a dacron graft in the pressurization test and an end-to-end anastomosis. *Journal of the Mechanical Behavior of Biomedical Materials 61* (2016), 36 – 44.

[38] Carew, E., Talman, E., Boughner, D., and Vesely, I. Quasi-linear viscoelastic theory applied to internal shearing of porcine aortic valve leaflets. *Journal of Biomechanical Engineering 121*, 4 (1999), 386–392.

[39] Carew, E. O., Garg, A., Barber, J. E., and Vesely, I. Stress Relaxation Preconditioning of Porcine Aortic Valves. *Annals of Biomedical Engineering 32*, 4 (2004), 563–572.

[40] Chaouat, M., Le Visage, C., Baille, W. E., Escoubet, B., Chaubet, F., Mateescu, M. A., and Letourneur, D. A Novel Cross-linked Poly(vinyl alcohol) (PVA) for Vascular Grafts. *Advanced Functional Materials 18*, 19 (2008), 2855–2861.

[41] Charitos, E. I., Takkenberg, J. J., Hanke, T., Gorski, A., Botha, C., Franke, U., Dodge-Khatami, A., Hoerer, J., Lange, R., Moritz, A., Ferrari-Kuehne, K., Hetzer, R., Huebler, M., Bogers, A. J., Stierle, U., Sievers, H.-H., and Hemmer, W. Reoperations on the pulmonary autograft and pulmonary homograft after the Ross procedure: An update on the German Dutch Ross Registry. *The Journal of Thoracic and Cardiovascular Surgery 144*, 4 (2012), 813 – 823.

[42] Chen, Y., and Fung, Y. Stress-strain history relations of rabbit mesentery in simple elongation. In *Biomechanical Symposium, ADM* (1973), vol. 2, pp. 9–10.

[43] Chilian, W. M., and Marcus, M. L. Phasic coronary blood flow velocity in intramural and epicardial coronary arteries. *Circulation Research 50*, 6 (1982), 775–781.

[44] Chow, M.-J., Turcotte, R., Lin, C. P., and Zhang, Y. Arterial extracellular matrix: A mechanobiological study of the contributions and interactions of elastin and collagen. *Biophysical Journal 106*, 12 (2014), 2684–2692.

[45] Chu, K. C., and Rutt, B. K. Polyvinyl alcohol cryogel: An ideal phantom material for MR studies of arterial flow and elasticity. *Magnetic Resonance in Medicine 37*, 2 (1997), 314–319.

[46] Chung, J., Lachapelle, K., Cartier, R., Mongrain, R., and Leask, R. L. Loss of mechanical directional dependency of the ascending aorta with severe medial degeneration. *Cardiovascular Pathology 26* (2017), 45 – 50.

[47] Chung, J., Lachapelle, K., Wener, E., Cartier, R., Varennes, B. D., Fraser, R., and Leask, R. L. Energy loss, a novel biomechanical parameter, correlates with aortic aneurysm size and histopathologic findings. *The Journal of Thoracic and Cardiovascular Surgery 148*, 3 (2014), 1082 – 1089. Proceedings of the 94th Annual Meeting of the American Association for Thoracic Surgery.

[48] Conconi, M. T., Borgio, L., Di Liddo, R., Sartore, L., Dalzoppo, D., Amistà, P., Lora, S., Parnigotto, P. P., and Grandi, C. Evaluation of vascular grafts based on polyvinyl alcohol cryogels. *Molecular Medicine Reports 10*, 3 (2014), 1329–1334.

[49] Cox, R. H. Passive mechanics and connective tissue composition of canine arteries. *American Journal of Physiology-Heart and Circulatory Physiology 234*, 5 (1978), H533–H541.

[50] Craiem, D., Graf, S., Armentano, R. L., and Barra, J. G. Vascular Smooth Muscle Activation Improves Aortic Compliance with Respect to Mechanical Loading. *Cardiovascular Engineering and Technology 3*, 1 (2012), 80–87.

[51] Dahl, S. L. M., Kypson, A. P., Lawson, J. H., Blum, J. L., Strader, J. T., Li, Y., Manson, R. J., Tente, W. E., DiBernardo, L., Hensley, M. T., Carter, R., Williams, T. P., Prichard, H. L., Dey, M. S., Begelman, K. G., and Niklason, L. E. Readily Available Tissue-Engineered Vascular Grafts. *Science Translational Medicine 3*, 68 (2011), 68ra9.

[52] Damme, H. V., Deprez, M., Creemers, E., and Limet, R. Intrinsic structural failure of polyester (Dacron) vascular grafts. A general review. *Acta Chirurgica Belgica 105*, 3 (2005), 249–255.

[53] Danpinid, A., Luo, J., Vappou, J., Terdtoon, P., and Konofagou, E. E. In vivo characterization of the aortic wall stress–strain relationship. *Ultrasonics 50*, 7 (2010), 654–665.

[54] David, T. E., David, C., Woo, A., and Manlhiot, C. The Ross procedure: outcomes at 20 years. *The Journal of Thoracic and Cardiovascular Surgery 147*, 1 (2014), 85–94.

[55] Davis, E. C. Stability of elastin in the developing mouse aorta: a quantitative radioautographic study. *Histochemistry 100*, 1 (Jul 1993), 17–26.

[56] De Bakey, M. E., Cooley, D. A., Crawford, E. S., and Morris Jr., G. C. Clinical application of a new flexible knitted dacron arterial substitute. *Archives of Surgery 77*, 5 (1958), 713–724.

[57] De Bakey, M. E., Jordan Jr., G. L., Abbott, J. P., Halpert, B., and O'Neal, R. M. The fate of dacron vascular grafts. *Archives of Surgery 89*, 5 (1964), 755–782.

[58] De Paulis, R., Scaffa, R., Maselli, D., Salica, A., Bellisario, A., and Weltert, L. A Third Generation of Ascending Aorta Dacron Graft: Preliminary Experience. *The Annals of Thoracic Surgery 85*, 1 (2008), 305–309.

[59] De Rosa, C., Auriemma, F., and Di Girolamo, R. *Kinetic Analysis of Cryotropic Gelation of Poly(Vinyl Alcohol)/Water Solutions by Small-Angle Neutron Scattering*. Springer International Publishing, 2014, pp. 159–197.

[60] Debes, J. C., and Fung, Y. C. Biaxial mechanics of excised canine pulmonary arteries. *American Journal of Physiology-Heart and Circulatory Physiology 269*, 2 (1995), H433–H442.

[61] Doehring, T. C., Carew, E. O., and Vesely, I. The effect of strain rate on the viscoelastic response of aortic valve tissue: A direct-fit approach. *Annals of Biomedical Engineering 32*, 2 (2004), 223–232.

[62] Domotenko, L., Lozinskii, V., Vainerman, Y., and Rogozhin, S. Effect of freezing conditions of dilute solutions of polyvinyl alcohol and conditions of defreezing samples on properties of cryogels obtained. *Polymer Science U.S.S.R. 30*, 8 (1988), 1758–1764.

[63] Duprey, A., Khanafer, K., Schlicht, M., Avril, S., Williams, D., and Berguer, R. In Vitro Characterisation of Physiological and Maximum Elastic Modulus of Ascending Thoracic Aortic Aneurysms Using Uniaxial Tensile Testing. *European Journal of Vascular and Endovascular Surgery 39*, 6 (2010), 700 – 707.

[64] El-Hamamsy, I., Eryigit, Z., Stevens, L.-M., Sarang, Z., George, R., Clark, L., Melina, G., Takkenberg, J. J., and Yacoub, M. H. Long-term outcomes after autograft versus homograft aortic root replacement in adults with aortic valve disease: a randomised controlled trial. *The Lancet 376*, 9740 (2010), 524 – 531.

[65] Emmott, A., El-Hamamsy, I., and L. Leask, R. Case Report: Histopathological and biomechanical properties of the aortic wall in 2 patients with chronic type A aortic dissection. *Cardiovascular Pathology 29* (2017), 48 – 52.

[66] Emmott, A., Garcia, J., Chung, J., Lachapelle, K., El-Hamamsy, I., Mongrain, R., Cartier, R., and Leask, R. L. Biomechanics of the Ascending Thoracic Aorta: A Clinical Perspective on Engineering Data. *Canadian Journal of Cardiology 32*, 1 (2016), 35 – 47.

[67] Etz, C. D., Homann, T., Silovitz, D., Bodian, C. A., Luehr, M., Di Luozzo, G., Plestis, K. A., and Griepp, R. B. Vascular graft replacement of the ascending and descending aorta: do Dacron grafts grow? *The Annals of Thoracic Surgery 84*, 4 (2007), 1206–1213.

[68] Fischer, G. M., and Llaurado, J. G. Collagen and Elastin Content in Canine Arteries Selected from Functionally Different Vascular Beds. *Circulation Research 19*, 2 (1966), 394–399.

[69] Fromageau, J., Gennisson, J., Schmitt, C., Maurice, R. L., Mongrain, R., and Cloutier, G. Estimation of polyvinyl alcohol cryogel mechanical properties with four ultrasound elastography methods and comparison with gold standard testings. *IEEE Transactions on Ultrasonics, Ferroelectrics, and Frequency Control 54*, 3 (2007), 498–509.

[70] Fung, Y.-C. *Stress-strain history relations of soft tissues in simple elongation*. Englewood, 1972, pp. 181–208.

[71] Fung, Y.-C. *Biomechanics: Mechanical Properties of Living Tissues*. Springer Science & Business Media, 1993.

[72] Furchgott, R. F., and Zawadzki, J. V. The obligatory role of endothelial cells in the relaxation of arterial smooth muscle by acetylcholine. *Nature 288*, 5789 (1980), 373–376.

[73] Gasser, T. C., Ogden, R. W., and Holzapfel, G. A. Hyperelastic modelling of arterial layers with distributed collagen fibre orientations. *Journal of The Royal Society Interface 3*, 6 (2006), 15–35.

[74] Geest, J. P. V., Sacks, M. S., and Vorp, D. A. The effects of aneurysm on the biaxial mechanical behavior of human abdominal aorta. *Journal of Biomechanics 39*, 7 (2006), 1324–1334.

[75] Gosline, J., Lillie, M., Carrington, E., Guerette, P., Ortlepp, C., and Savage, K. Elastic proteins: biological roles and mechanical properties. *Philosophical Transactions of the Royal Society of London B: Biological Sciences 357*, 1418 (2002), 121–132.

[76] Goto, M., and Kimoto, Y. Hysteresis and stress-relaxation of the blood vessels studied by a universal tensile testing instrument. *Japanese Journal of Physiology 16*, 2 (1966), 169–184.

[77] Greenwald, S., and Berry, C. Improving vascular grafts: the importance of mechanical and haemodynamic properties. *The Journal of Pathology 190*, 3 (2000), 292–299.

[78] Gundiah, N., Ratcliffe, M. B., and Pruitt, L. A. Determination of strain energy function for arterial elastin: Experiments using histology and mechanical tests. *Journal of Biomechanics 40*, 3 (2007), 586–594.

[79] Gundiah, N., Ratcliffe, M. B., and Pruitt, L. A. The biomechanics of arterial elastin. *Journal of the Mechanical Behavior of Biomedical Materials 2*, 3 (2009), 288–296.

[80] Guo, D.-C., Regalado, E. S., Minn, C., Tran-Fadulu, V., Coney, J., Cao, J., Wang, M., Robert, K. Y., Estrera, A. L., Safi, H. J., et al. Familial Thoracic

Aortic Aneurysms and Dissections: Identification of a Novel Locus for Stable Aneurysms with a Low Risk for Progression to Aortic Dissection. *Circulation Cardiovascular Genetics 4* (2011), 36–42.

[81] Hanson, S. R., Kotze, H. F., Savage, B., and Harker, L. A. Platelet interactions with Dacron vascular grafts. A model of acute thrombosis in baboons. *Arteriosclerosis 5*, 6 (1985), 595–603.

[82] Harkness, M. L., Harkness, R., and McDonald, D. The collagen and elastin content of the arterial wall in the dog. *Proceedings of the Royal Society of London B: Biological Sciences 146*, 925 (1957), 541–551.

[83] Harris, E. J., Shumacker Jr, H. B., Siderys, H., Moore, T. C., and Grice, P. F. Pliable plastic aortic grafts: Experimental comparison of a number of materials. *A.M.A. Archives of Surgery 71*, 3 (1955), 449–459.

[84] Hasegawa, M., and Azuma, T. Mechanical properties of synthetic arterial grafts. *Journal of Biomechanics 12*, 7 (1979), 509 – 517.

[85] Hass, G. Elastic tissue. II. A study of the elasticity and tensile strength of elastic tissue isolated from the human aorta. *Archives of Pathology 34* (1942), 971 – 981.

[86] Hassan, C. M., and Peppas, N. A. *Structure and Applications of Poly(vinyl alcohol) Hydrogels Produced by Conventional Crosslinking or by Freezing/Thawing Methods*. Springer Berlin Heidelberg, Berlin, Heidelberg, 2000, pp. 37–65.

[87] Hassan, C. M., and Peppas, N. A. Structure and Morphology of Freeze/Thawed PVA Hydrogels. *Macromolecules 33*, 7 (2000), 2472–2479.

[88] Hayashi, T., Nakayama, Y., Tsumura, K., Yoshimaru, K., and Ueda, H. Reflection in the arterial system and the risk of coronary heart disease. *American Journal of Hypertension 15*, 5 (2002), 405–409.

[89] Hellenthal, F. A., Geenen, I. L., Teijink, J. A., Heeneman, S., and Schurink, G. W. H. Histological features of human abdominal aortic aneurysm are not related to clinical characteristics. *Cardiovascular Pathology 18*, 5 (2009), 286–293.

[90] Herlihy, J. T., and Murphy, R. A. Length-tension relationship of smooth muscle of the hog carotid artery. *Circulation Research 33*, 3 (1973), 275–283.

[91] Hesse, D., Cozart, D., Szymik, B., and Nichols, R. Anatomy and Physiology II Lab Manual (UGA).

[92] Hibino, N., McGillicuddy, E., Matsumura, G., Ichihara, Y., Naito, Y., Breuer, C., and Shinoka, T. Late-term results of tissue-engineered vascular grafts in humans. *The Journal of Thoracic and Cardiovascular Surgery 139*, 2 (2010), 431–436.

[93] Hilden, T. The influence of arterial compliance on diastolic blood pressure and its relation to cardiovascular events. *Journal of Human Hypertension 5*, 3 (1991), 131–135.

[94] Hoerstrup, S. P., Cummings MRCS, I., Lachat, M., Schoen, F. J., Jenni, R., Leschka, S., Neuenschwander, S., Schmidt, D., Mol, A., Gunter, C., et al. Functional growth in tissue-engineered living, vascular grafts: follow-up at 100 weeks in a large animal model. *Circulation 114*, 1_supplement (2006), I159–I166.

[95] Hosoda, Y., Kawano, K., Yamasawa, F., Ishii, T., Shibata, T., and Inayama, S. Age-Dependent Changes of Collagen and Elastin Content in Human Aorta and Pulmonary Artery. *Angiology 35*, 10 (1984), 615–621.

[96] How, T. V., and Annis, D. Viscoelastic behavior of polyurethane vascular prostheses. *Journal of Biomedical Materials Research 21*, 9 (1987), 1093–1108.

[97] Huglin, M. R. Hydrogels in medicine and pharmacy. *British Polymer Journal 21*, 2 (1989), 184.

[98] Imura, T., Yamamoto, K., Satoh, T., Kanamori, K., Mikami, T., and Yasuda, H. In vivo viscoelastic behavior in the human aorta. *Circulation Research 66*, 5 (1990), 1413–1419.

[99] Ioannou, C., Stergiopulos, N., Katsamouris, A., Startchik, I., Kalangos, A., Licker, M., Westerhof, N., and Morel, D. Hemodynamics induced after acute reduction of proximal thoracic aorta compliance. *European Journal of Vascular and Endovascular Surgery 26*, 2 (2003), 195–204.

[100] Ioannou, C. V., Morel, D. R., Katsamouris, A. N., Katranitsa, S., Startchik, I., Kalangos, A., Westerhof, N., and Stergiopulos, N. Left ventricular hypertrophy induced by reduced aortic compliance. *Journal of Vascular Research 46*, 5 (2009), 417–425.

[101] Ishibashi, H., Sunamura, M., and Karino, T. Flow patterns and preferred sites of intimal thickening in end-to-end anastomosed vessels. *Surgery 117*, 4 (1995), 409–420.

[102] Jiang, H., Campbell, G., Boughner, D., Wan, W.-K., and Quantz, M. Design and manufacture of a polyvinyl alcohol (PVA) cryogel tri-leaflet heart valve prosthesis. *Medical Engineering & Physics 26*, 4 (2004), 269 – 277.

[103] Kajiya, F., Tomonaga, G., Tsujioka, K., Ogasawara, Y., and Nishihara, H. Evaluation of local blood flow velocity in proximal and distal coronary arteries by laser doppler method. *Journal of Biomechanical Engineering 107*, 1 (1985), 10–15.

[104] Kapil, V., Sobotka, P. A., Saxena, M., Mathur, A., Knight, C., Dolan, E., Stanton, A., and Lobo, M. D. Central iliac arteriovenous anastomosis for hypertension:

targeting mechanical aspects of the circulation. *Current Hypertension Reports 17*, 9 (2015), 73.

[105] Kawamura, M., Ogino, H., Matsuda, H., Minatoya, K., Sasaki, H., and Kitamura, S. Late-stage, nonanastomotic rupture of double-velour Dacron graft after descending aortic replacement. *The Journal of Thoracic and Cardiovascular Surgery 132*, 4 (2006), 961–962.

[106] Kawata, M., Morota, T., Takamoto, S., Kubota, H., and Kitahori, K. Non-anastomotic rupture in the guideline of a Dacron thoracic aortic graft. *Journal of Vascular Surgery 42*, 3 (2005), 573.

[107] Kelly, R. P., Tunin, R., and Kass, D. A. Effect of reduced aortic compliance on cardiac efficiency and contractile function of in situ canine left ventricle. *Circulation Research 71*, 3 (1992), 490–502.

[108] Kidson, I. The effect of wall mechanical properties on patency of arterial grafts. *Annals of the Royal College of Surgeons of England 65*, 1 (1983), 24.

[109] Kim, S. Y., Hinkamp, T. J., Jacobs, W. R., Lichtenberg, R. C., Posniak, H., and Pifarré, R. Effect of an inelastic aortic synthetic vascular graft on exercise hemodynamics. *The Annals of Thoracic Surgery 59*, 4 (1995), 981–989.

[110] King, D. M., Moran, C. M., McNamara, J. D., Fagan, A. J., and Browne, J. E. Development of a vessel-mimicking material for use in anatomically realistic Doppler flow phantoms. *Ultrasound in Medicine & Biology 37*, 5 (2011), 813–826.

[111] Kobayashi, M. A study of Polyvinyl Alcohol–Hydrogel (PVA–H) artificial meniscus in vivo. *Bio-Medical Materials & Engineering 14*, 4 (2004), 505–515.

[112] Kobayashi, M., and Hyu, H. S. Development and evaluation of polyvinyl alcohol-hydrogels as an artificial atrticular cartilage for orthopedic implants. *Materials 3*, 4 (2010), 2753–2771.

[113] Kohandel, M., Sivaloganathan, S., and Tenti, G. Estimation of the quasi-linear viscoelastic parameters using a genetic algorithm. *Mathematical and Computer Modelling 47*, 3 (2008), 266 – 270.

[114] Kohler, T. R., Kirkman, T. R., and Clowes, A. W. The effect of rigid external support on vein graft adaptation to the arterial circulation. *Journal of Vascular Surgery 9*, 2 (1989), 277–285.

[115] Kosukegawa, H., Mamada, K., Kuroki, K., Liu, L., Inoue, K., Hayase, T., and Ohta, M. Measurements of Dynamic Viscoelasticity of Poly (vinyl alcohol) Hydrogel for the Development of Blood Vessel Biomodeling. *Journal of Fluid Science and Technology 3*, 4 (2008), 533–543.

[116] Kouchoukos, N. T., Masetti, P., Nickerson, N. J., Castner, C. F., Shannon, W. D., and Dvila-Romn, V. G. The Ross procedure: Long-term clinical and echocardiographic follow-up. *The Annals of Thoracic Surgery 78*, 3 (2004), 773 – 781.

[117] Krüger, T., Conzelmann, L. O., Bonser, R. S., Borger, M. A., Czerny, M., Wildhirt, S., Carrel, T., Mohr, F. W., Schlensak, C., and Weigang, E. Acute aortic dissection type a. *British Journal of Surgery 99*, 10 (2012), 1331–1344.

[118] Langewouters, G., Wesseling, K., and Goedhard, W. The static elastic properties of 45 human thoracic and 20 abdominal aortas in vitro and the parameters of a new model. *Journal of Biomechanics 17*, 6 (1984), 425 – 435.

[119] Langewouters, G., Wesseling, K., and Goedhard, W. The pressure dependent dynamic elasticity of 35 thoracic and 16 abdominal human aortas in vitro described by a five component model. *Journal of Biomechanics 18*, 8 (1985), 613 – 620.

[120] Lee, J. M., and Wilson, G. J. Anisotropic tensile viscoelastic properties of vascular graft materials tested at low strain rates. *Biomaterials 7*, 6 (1986), 423 – 431.

[121] Leyh, R. G., Schmidtke, C., Sievers, H.-H., and Yacoub, M. H. Opening and closing characteristics of the aortic valve after different types of valve-preserving surgery. *Circulation 100*, 21 (1999), 2153–2160.

[122] L'Heureux, N., Dusserre, N., Konig, G., Victor, B., Keire, P., Wight, T. N., Chronos, N. A., Kyles, A. E., Gregory, C. R., Hoyt, G., et al. Human tissue-engineered blood vessels for adult arterial revascularization. *Nature Medicine 12*, 3 (2006), 361.

[123] L'Heureux, N., Germain, L., Labb, R., and Auger, F. A. In vitro construction of a human blood vessel from cultured vascular cells: A morphologic study. *Journal of Vascular Surgery 17*, 3 (1993), 499 – 509.

[124] L'Heureux, N., Pquet, S., Labb, R., Germain, L., and Auger, F. A. A completely biological tissue-engineered human blood vessel. *The FASEB Journal 12*, 1 (1998), 47–56.

[125] Lillie, M., and Gosline, J. Mechanical properties of elastin along the thoracic aorta in the pig. *Journal of Biomechanics 40*, 10 (2007), 2214–2221.

[126] Loeys, B. L., Dietz, H. C., Braverman, A. C., Callewaert, B. L., De Backer, J., Devereux, R. B., Hilhorst-Hofstee, Y., Jondeau, G., Faivre, L., Milewicz, D. M., Pyeritz, R. E., Sponseller, P. D., Wordsworth, P., and De Paepe, A. M. The revised Ghent nosology for the Marfan syndrome. *Journal of Medical Genetics 47*, 7 (2010), 476–485.

[127] Lozinsky, V., and Plieva, F. Poly(vinyl alcohol) cryogels employed as matrices for cell immobilization. 3. Overview of recent research and developments. *Enzyme and Microbial Technology 23*, 3 (1998), 227 – 242.

[128] Lozinsky, V. I. Cryotropic gelation of poly(vinyl alcohol) solutions. *Russian Chemical Reviews 67*, 7 (1998), 573–586.

[129] Lozinsky, V. I. Cryogels on the basis of natural and synthetic polymers: preparation, properties and application. *Russian Chemical Reviews 71*, 6 (2002), 489.

[130] Lozinsky, V. I., Zubov, A. L., Savina, I. N., and Plieva, F. M. Study of cryostructuration of polymer systems. XIV. Poly(vinyl alcohol) cryogels: Apparent yield of the freezethaw-induced gelation of concentrated aqueous solutions of the polymer. *Journal of Applied Polymer Science 77*, 8 (2000), 1822–1831.

[131] Maeta, H., and Hori, M. Effects of a Lack of Aortic "Windkessel" Properties on the Left Ventricle. *Japanese Circulation Journal 49*, 2 (1985), 232.

[132] Maitra, J., and Shukla, V. K. Cross-linking in Hydrogels - A Review. *American Journal of Polymer Science 4*, 2 (2014), 25–31.

[133] Matsumura, G., Isayama, N., Matsuda, S., Taki, K., Sakamoto, Y., Ikada, Y., and Yamazaki, K. Long-term results of cell-free biodegradable scaffolds for in situ tissue engineering of pulmonary artery in a canine model. *Biomaterials 34*, 27 (2013), 6422 – 6428.

[134] Matsumura, G., Nitta, N., Matsuda, S., Sakamoto, Y., Isayama, N., Yamazaki, K., and Ikada, Y. Long-Term Results of Cell-Free Biodegradable Scaffolds for In Situ Tissue-Engineering Vasculature: In a Canine Inferior Vena Cava Model. *PLOS ONE 7*, 4 (04 2012), 1–9.

[135] Maxwell, J. A., and Anliker, M. The Dissipation and Dispersion of Small Waves in Arteries and Veins with Viscoelastic Wall Properties. *Biophysical Journal 8*, 8 (1968), 920 – 950.

[136] Mehigan, D., Fitzpatrick, B., Browne, H., and Bouchier-Hayes, D. Is compliance mismatch the major cause of anastomotic arterial aneurysms? Analysis of 42 cases. *The Journal of Cardiovascular Surgery 26*, 2 (1985), 147–150.

[137] Menacho, J., Rotllant, L., Molins, J. J., Reyes, G., García-Granada, A. A., Balcells, M., and Martorell, J. Arterial pulse attenuation prediction using the decaying rate of a pressure wave in a viscoelastic material model. *Biomechanics and Modeling in Mechanobiology 17*, 2 (2018), 589–603.

[138] Millon, L., and Wan, W. The polyvinyl alcohol–bacterial cellulose system as a new nanocomposite for biomedical applications. *Journal of Biomedical Materials Research Part B: Applied Biomaterials 79*, 2 (2006), 245–253.

[139] Millon, L. E., Mohammadi, H., and Wan, W. K. Anisotropic polyvinyl alcohol hydrogel for cardiovascular applications. *Journal of Biomedical Materials Research Part B: Applied Biomaterials 79B*, 2 (2006), 305–311.

[140] Millon, L. E., Padavan, D. T., Hamilton, A. M., Boughner, D. R., and Wan, W. Exploring cell compatibility of a fibronectin-functionalized physically crosslinked poly(vinyl alcohol) hydrogel. *Journal of Biomedical Materials Research Part B: Applied Biomaterials 100*, 1 (2012), 1–10.

[141] Mitchell, G. F. Arterial Stiffness and Hypertension: Chicken or Egg? *Hypertension 64*, 2 (2014), 210.

[142] Mohammadi, H., Boughner, D., Millon, L., and Wan, W. Design and simulation of a poly(vinyl alcohol)bacterial cellulose nanocomposite mechanical aortic heart valve prosthesis. *Proceedings of the Institution of Mechanical Engineers, Part H: Journal of Engineering in Medicine 223*, 6 (2009), 697–711.

[143] Mohan, D., and Melvin, J. W. Failure properties of passive human aortic tissue. IIBiaxial tension tests. *Journal of Biomechanics 16*, 1 (1983), 39–44.

[144] Mori, Y., Tokura, H., and Yoshikawa, M. Properties of hydrogels synthesized by freezing and thawing aqueous polyvinyl alcohol solutions and their applications. *Journal of Materials Science 32*, 2 (1997), 491–496.

[145] Morinaga, K., Okadome, K., Kuroki, M., Miyazaki, T., Muto, Y., and Inokuchi, K. Effect of wall shear stress on intimal thickening of arterially transplanted autogenous veins in dogs. *Journal of Vascular Surgery 2*, 3 (1985), 430–433.

[146] Morita, S., Asou, T., Kuboyama, I., Harasawa, Y., Sunagawa, K., and Yasui, H. Inelastic vascular prosthesis for proximal aorta increases pulsatile arterial load and causes left ventricular hypertrophy in dogs. *The Journal of Thoracic and Cardiovascular Surgery 124*, 4 (2002), 768 – 774.

[147] Nagano, N., Cartier, R., Zigras, T., Mongrain, R., and Leask, R. L. Mechanical properties and microscopic findings of a Dacron graft explanted 27 years after coarctation repair. *The Journal of Thoracic and Cardiovascular Surgery 134*, 6 (2007), 1577–1578.

[148] Nekouzadeh, A., Pryse, K. M., Elson, E. L., and Genin, G. M. A simplified approach to quasi-linear viscoelastic modeling. *Journal of Biomechanics 40*, 14 (2007), 3070–3078.

[149] Niklason, L. E., Gao, J., Abbott, W. M., Hirschi, K. K., Houser, S., Marini, R., and Langer, R. Functional Arteries Grown in Vitro. *Science 284*, 5413 (1999), 489–493.

[150] Niklason, L. E., and Langer, R. S. Advances in tissue engineering of blood vessels and other tissues. *Transplant Immunology 5*, 4 (1997), 303–306.

[151] Nuttelman, C. R., Mortisen, D. J., Henry, S. M., and Anseth, K. S. Attachment of fibronectin to poly(vinyl alcohol) hydrogels promotes NIH3T3 cell adhesion, proliferation, and migration. *Journal of Biomedical Materials Research 57*, 2 (2001), 217–223.

[152] Ohtsuka, S., Kakihana, M., Watanabe, H., and Sugishita, Y. Chronically decreased aortic distensibility causes deterioration of coronary perfusion during increased left ventricular contraction. *Journal of the American College of Cardiology 24*, 5 (1994), 1406 – 1414.

[153] Okamoto, R. J., Wagenseil, J. E., DeLong, W. R., Peterson, S. J., Kouchoukos, N. T., and Sundt, T. M. Mechanical Properties of Dilated Human Ascending Aorta. *Annals of Biomedical Engineering 30*, 5 (2002), 624–635.

[154] Okuhn, S. P., Connelly, D. P., Calakos, N., Ferrell, L., Man-Xiang, P., and Goldstone, J. Does compliance mismatch alone cause neointimal hyperplasia? *Journal of Vascular Surgery 9*, 1 (1989), 35–45.

[155] O'Rourke, M. Arterial stiffness, systolic blood pressure, and logical treatment of arterial hypertension. *Hypertension 15*, 4 (1990), 339–347.

[156] Paasche, P., Kinley, C., Dolan, F., Gozna, E., and Marble, A. Consideration of suture line stresses in the selection of synthetic grafts for implantation. *Journal of Biomechanics 6*, 3 (1973), 253 – 259.

[157] Pashneh-Tala, S., MacNeil, S., and Claeyssens, F. The Tissue-Engineered Vascular Graft-Past, Present, and Future. *Tissue Engineering Part B: Reviews 22*, 1 (2015), 68–100.

[158] Pazos, V., Mongrain, R., and Tardif, J. Polyvinyl alcohol cryogel: Optimizing the parameters of cryogenic treatment using hyperelastic models. *Journal of the Mechanical Behavior of Biomedical Materials 2*, 5 (2009), 542 – 549.

[159] Peppas, N. A. Turbidimetric studies of aqueous poly(vinyl alcohol) solutions. *Die Makromolekulare Chemie: Macromolecular Chemistry and Physics 176*, 11 (1975), 3433–3440.

[160] Peterson, L. H., Jensen, R. E., and Parnell, J. Mechanical Properties of Arteries in Vivo. *Circulation Research 8*, 3 (1960), 622–639.

[161] Pourdeyhimi, B., and Wagner, D. On the correlation between the failure of vascular grafts and their structural and material properties: a critical analysis. *Journal of Biomedical Materials Research 20*, 3 (1986), 375–409.

[162] Pratt, G. H. Use of Teflon in replacement of aortic and arterial segments: Experimental and clinical results compared with homografts and other materials. *The American Journal of Surgery 100*, 3 (1960), 389–395.

[163] Quint, C., Arief, M., Muto, A., Dardik, A., and Niklason, L. E. Allogeneic human tissue-engineered blood vessel. *Journal of Vascular Surgery 55*, 3 (2012), 790–798.

[164] Quint, C., Kondo, Y., Manson, R. J., Lawson, J. H., Dardik, A., and Niklason, L. E. Decellularized tissue-engineered blood vessel as an arterial conduit. *Proceedings of the National Academy of Sciences* (2011), 9214–9219.

[165] R, W., GJ, L., J, M., and WM, A. Matched elastic properties and successful arterial grafting. *Archives of Surgery 115*, 10 (1980), 1166–1169.

[166] Remington, J. W. Hysteresis loop behavior of the aorta and other extensible tissues. *American Journal of Physiology 180*, 1 (1954), 83–95.

[167] Rhee, K., and Tarbell, J. M. A study of the wall shear rate distribution near the end-to-end anastomosis of a rigid graft and a compliant artery. *Journal of Biomechanics 27*, 3 (1994), 329–338.

[168] Rhodin, J. A. G. Architecture of the Vessel Wall, Handbook of Physiology, The Cardiovascular System. *Bethesda, MD: The American Physiological Society 2* (1980), 1–31.

[169] Roach, M. R., and Burton, A. C. The reason for the shape of the distensibility curves of arteries. *Canadian Journal of Biochemistry and Physiology 35*, 8 (1957), 681–690.

[170] Roselli, E. E., Idrees, J., Greenberg, R. K., Johnston, D. R., and Lytle, B. W. Endovascular stent grafting for ascending aorta repair in high-risk patients. *The Journal of Thoracic and Cardiovascular Surgery 149*, 1 (2015), 144 – 154.

[171] Ross, D. N. Replacement of aortic and mitral valves with a pulmonary autograft. *The Lancet 290*, 7523 (1967), 956–958.

[172] Roy, C. S. The Elastic Properties of the Arterial Wall. *The Journal of Physiology 3*, 2 (1881), 125–159.

[173] Saito, M., Ikenaga, Y., Matsukawa, M., Watanabe, Y., Asada, T., and Lagrée, P.-Y. One-dimensional model for propagation of a pressure wave in a model of the human arterial network: Comparison of theoretical and experimental results. *Journal of Biomechanical Engineering 133*, 12 (2011), 121005–1–121005–9.

[174] Salvucci, F. P., Schiavone, J., Craiem, D., and Barra, J. G. Arterial wall mechanics as a function of heart rate: role of vascular smooth muscle. *Journal of Physics: Conference Series 90*, 1 (2007), 012010–1–012010–7.

[175] Sandoo, A., van Zanten, J. J. V., Metsios, G. S., Carroll, D., and Kitas, G. D. The Endothelium and Its Role in Regulating Vascular Tone. *The Open Cardiovascular Medicine Journal 4* (2010), 302.

[176] Shadwick, R. E. Mechanical design in arteries. *Journal of Experimental Biology 202*, 23 (1999), 3305–3313.

[177] Shadwick, R. E., and Gosline, J. M. Mechanical properties of the octopus aorta. *Journal of Experimental Biology 114*, 1 (1985), 259–284.

[178] Shapiro, S., Endicott, S., Province, M., Pierce, J., and Campbell, E. Marked longevity of human lung parenchymal elastic fibers deduced from prevalence of d-aspartate and nuclear weapons-related radiocarbon. *The Journal of Clinical Investigation 87*, 5 (1991), 1828–1834.

[179] Shinoka, T., Matsumura, G., Hibino, N., Naito, Y., Watanabe, M., Konuma, T., Sakamoto, T., Nagatsu, M., and Kurosawa, H. Midterm clinical result of tissue-engineered vascular autografts seeded with autologous bone marrow cells. *The Journal of Thoracic and Cardiovascular Surgery 129*, 6 (2005), 1330–1338.

[180] Sokolis, D. P. Passive mechanical properties and structure of the aorta: segmental analysis. *Acta Physiologica 190*, 4 (2007), 277–289.

[181] Sokolis, D. P., Boudoulas, H., and Karayannacos, P. E. Assessment of the aortic stressstrain relation in uniaxial tension. *Journal of Biomechanics 35*, 9 (2002), 1213 – 1223.

[182] Stammen, J. A., Williams, S., Ku, D. N., and Guldberg, R. E. Mechanical properties of a novel PVA hydrogel in shear and unconfined compression. *Biomaterials 22*, 8 (2001), 799–806.

[183] Stauffer, S. R., and Peppast, N. A. Poly(vinyl alcohol) hydrogels prepared by freezing-thawing cyclic processing. *Polymer 33*, 18 (1992), 3932–3936.

[184] Stefanadis, C., Stratos, C., Vlachopoulos, C., Marakas, S., Boudoulas, H., Kallikazaros, I., Tsiamis, E., Toutouzas, K., Sioros, L., and Toutouzas, P. Pressure-Diameter Relation of the Human Aorta. *Circulation 92*, 8 (1995), 2210–2219.

[185] Stewart, S. F., and Lyman, D. J. Effects of a vascular graft/natural artery compliance mismatch on pulsatile flow. *Journal of Biomechanics 25*, 3 (1992), 297–310.

[186] Tadavarthy, S. M., MOLLER, J. H., and AMPLATZ, K. Polyvinyl alcohol (Ivalon)a new embolic material. *American Journal of Roentgenology 125*, 3 (1975), 609–616.

[187] Tai, N. R., Salacinski, H. J., Edwards, A., Hamilton, G., and Seifalian, A. Compliance properties of conduits used in vascular reconstruction. *British Journal of Surgery 87*, 11 (2000), 1516–1524.

[188] Tian, D., Rahnavardi, M., and Yan, T. D. Aortic valve sparing operations in aortic root aneurysms: remodeling or reimplantation? *Annals of Cardiothoracic Surgery 2*, 1 (2013), 44.

[189] Tiwari, A., Cheng, K.-S., Salacinski, H., Hamilton, G., and Seifalian, A. Improving the patency of vascular bypass grafts: The role of suture materials and surgical

techniques on reducing anastomotic compliance mismatch. *European Journal of Vascular and Endovascular Surgery 25*, 4 (2003), 287 – 295.

[190] Treiman, G. S., Weaver, F. A., Cossman, D. V., Foran, R. F., Cohen, J. L., Levin, P. M., and Treiman, R. L. Anastomotic false aneurysms of the abdominal aorta and the iliac arteries. *Journal of Vascular Surgery 8*, 3 (1988), 268–273.

[191] Tremblay, D., Zigras, T., Cartier, R., Leduc, L., Butany, J., Mongrain, R., and Leask, R. L. A comparison of mechanical properties of materials used in aortic arch reconstruction. *The Annals of Thoracic Surgery 88*, 5 (2009), 1484–1491.

[192] Trieu, H., and Qutubuddin, S. Poly(vinyl alcohol) hydrogels: 2. Effects of processing parameters on structure and properties. *Polymer 36*, 13 (1995), 2531 – 2539.

[193] Trubel, W., Schima, H., Moritz, A., Raderer, F., Windisch, A., Ullrich, R., Windberger, U., Losert, U., and Polterauer, P. Compliance Mismatch and Formation of Distal Anastomotic Intimal Hyperplasia in Externally Stiffened and Lumen-Adapted Venous Grafts. *European Journal of Vascular and Endovascular Surgery 10*, 4 (1995), 415 – 423.

[194] Tsamis, A., Krawiec, J. T., and Vorp, D. A. Elastin and collagen fibre microstructure of the human aorta in ageing and disease: a review. *Journal of The Royal Society Interface 10*, 83 (2013).

[195] Tubaldi, E., Païdoussis, M. P., and Amabili, M. Nonlinear dynamics of Dacron aortic prostheses conveying pulsatile flow. *Journal of Biomechanical Engineering 140*, 6 (2018), 061004–1–061004–12.

[196] Um, K., Mcclure, G., Belley-Cote, E., Gupta, S., Bouhout, I., Lortie, H., Alraddadi, H., Alsagheir, A., Bossard, M., Mcintyre, W., et al. Hemodynamic outcomes of the Ross procedure versus other aortic valve replacement: a systematic review and meta-analysis. *The Journal of Cardiovascular Surgery 59*, 3 (2018), 462–470.

[197] Urschel, C. W., Covell, J. W., Sonnenblick, E. H., Ross Jr, J., and Braunwald, E. Effects of decreased aortic compliance on performance of the left ventricle. *American Journal of Physiology 214*, 2 (1968), 298–304.

[198] Valdez-Jasso, D., Bia, D., Zócalo, Y., Armentano, R. L., Haider, M. A., and Olufsen, M. S. Linear and nonlinear viscoelastic modeling of aorta and carotid pressure–area dynamics under in vivo and ex vivo conditions. *Annals of Biomedical Engineering 39*, 5 (2011), 1438–1456.

[199] Vardoulis, O., Coppens, E., Martin, B., Reymond, P., Tozzi, P., and Stergiopulos, N. Impact of Aortic Grafts on Arterial Pressure: A Computational Fluid Dynamics Study. *European Journal of Vascular and Endovascular Surgery 42*, 5 (2011), 704–710.

[200] Voorhees Jr, A. B., and Alfred Jaretzki III, A. H. B. The Use of Tubes Constructed from Vinyon N Cloth in Bridging Arterial Defects: A Preliminary Report. *Annals of Surgery 135*, 3 (1952), 332.

[201] Vrana, N. E., Liu, Y., McGuinness, G. B., and Cahill, P. A. Characterization of Poly(vinyl alcohol)/Chitosan Hydrogels as Vascular Tissue Engineering Scaffolds. *Macromolecular Symposia 269*, 1 (2008), 106–110.

[202] Walden, R., Gilbert, J., Megerman, J., and Abbott, W. M. Matched elastic properties and successful arterial grafting. *Archives of Surgery 115*, 10 (1980), 1166–1169.

[203] Wan, W., Campbell, G., Zhang, Z., Hui, A., and Boughner, D. Optimizing the tensile properties of polyvinyl alcohol hydrogel for the construction of a bioprosthetic heart valve stent. *Journal of Biomedical Materials Research 63*, 6 (2002), 854–861.

[204] Wang, B. H., and Campbell, G. Formulations of polyvinyl alcohol cryogel that mimic the biomechanical properties of soft tissues in the natural lumbar intervertebral disc. *Spine 34*, 25 (2009), 2745–2753.

[205] Watanabe, H., Ohtsuka, S., Kakihana, M., and Sugishita, Y. Coronary circulation in dogs with an experimental decrease in aortic compliance. *Journal of the American College of Cardiology 21*, 6 (1993), 1497–1506.

[206] Watton, P. N., Ventikos, Y., and Holzapfel, G. A. Modelling the mechanical response of elastin for arterial tissue. *Journal of Biomechanics 42*, 9 (2009), 1320–1325.

[207] Weber, T., Auer, J., O'Rourke, M. F., Kvas, E., Lassnig, E., Berent, R., and Eber, B. Arterial stiffness, wave reflections, and the risk of coronary artery disease. *Circulation 109*, 2 (2004), 184–189.

[208] Weinberg, C., and Bell, E. A blood vessel model constructed from collagen and cultured vascular cells. *Science 231*, 4736 (1986), 397–400.

[209] Weizsacker, H. W., and Pinto, J. G. Isotropy and anisotropy of the arterial wall. *Journal of Biomechanics 21*, 6 (1988), 477 – 487.

[210] Wells, S. M., Langille, B. L., Lee, J. M., and Adamson, S. L. Determinants of mechanical properties in the developing ovine thoracic aorta. *American Journal of Physiology-Heart and Circulatory Physiology 277*, 4 (1999), H1385–H1391.

[211] Wertheim, G. Mémoire sur l'élasticité et la cohésion des principaux tissus du corps humain. *Annales de Chimie et de Physique 21* (1847), 385–414.

[212] Westerhof, N., and Noordergraaf, A. Arterial viscoelasticity: A generalized model. Effect on input impedance and wave travel in the systematic tree. *Journal of Biomechanics 3*, 3 (1970), 357–370.

[213] Woo, S. Mechanical properties of tendons and ligaments. I. Quasi-static and nonlinear viscoelastic properties. *Biorheology 19*, 3 (1982), 385.

[214] Yamaguchi, S., Asakura, T., Miura, S., Ohki, T., Kanaoka, Y., Ohta, H., Yajima, N., and Nakaya, M. Nonanastomotic rupture of thoracic aortic Dacron graft treated by endovascular stent graft placement. *General Thoracic and Cardiovascular Surgery 61*, 7 (2013), 414–416.

[215] Yokota, T., Ichikawa, H., Matsumiya, G., Kuratani, T., Sakaguchi, T., Iwai, S., Shirakawa, Y., Torikai, K., Saito, A., Uchimura, E., et al. In situ tissue regeneration using a novel tissue-engineered, small-caliber vascular graft without cell seeding. *The Journal of Thoracic and Cardiovascular Surgery 136*, 4 (2008), 900–907.

[216] Yokoyama, F., Masada, I., Shimamura, K., Ikawa, T., and Monobe, K. Morphology and structure of highly elastic poly(vinyl alcohol) hydrogel prepared by repeated freezing-and-melting. *Colloid and Polymer Science 264*, 7 (1986), 595–601.

[217] Zajaczkowski, M. B., Cukierman, E., Galbraith, C. G., and Yamada, K. M. Cell-Matrix Adhesions on Poly(vinyl alcohol) Hydrogels. *Tissue Engineering 9*, 3 (2003), 525–533.

[218] Zamir, M. Mechanics of blood supply to the heart: wave reflection effects in a right coronary artery. *Proceedings of the Royal Society of London B: Biological Sciences 265*, 1394 (1998), 439–444.

[219] Zou, Y., and Zhang, Y. The orthotropic viscoelastic behavior of aortic elastin. *Biomechanics and Modeling in Mechanobiology 10*, 5 (2011), 613–625.